Timely Closure of the Prospore Membrane Requires *SPS1* and *SPO77* in *Saccharomyces cerevisiae*

Scott M. Paulissen, Christian J. Slubowski,[1] Joseph M. Roesner,[2] and Linda S. Huang[3]
Department of Biology, University of Massachusetts, Boston, Massachusetts 02125
ORCID ID: 0000-0002-9033-4391 (L.S.H.)

ABSTRACT During sporulation in *Saccharomyces cerevisiae*, a double lipid bilayer called the prospore membrane is formed *de novo*, growing around each meiotic nucleus and ultimately closing to create four new cells within the mother cell. Here we show that *SPS1*, which encodes a kinase belonging to the germinal center kinase III family, is involved in prospore membrane development and is required for prospore membrane closure. We find that *SPS1* genetically interacts with *SPO77* and see that loss of either gene disrupts prospore membrane closure in a similar fashion. Specifically, cells lacking *SPS1* and *SPO77* produce hyperelongated prospore membranes from which the leading edge protein complex is not removed from the prospore membrane in a timely fashion. The *SPS1*/*SPO77* pathway is required for the proper phosphorylation and stability of Ssp1, a member of the leading edge protein complex that is removed and degraded when the prospore membrane closes. Genetic dissection of prospore membrane closure finds *SPS1* and *SPO77* act in parallel to a previously described pathway of prospore membrane closure that involves *AMA1*, an activator of the meiotic anaphase promoting complex.

KEYWORDS prospore membrane; meiotic exit; anaphase promoting complex; sporulation; cytokinesis; germinal center kinase

BIOLOGICAL membranes provide a barrier for inhibiting the flow of materials between a cell and its surroundings and for compartmentalizing the contents of the various organelles within a cell. The size and shape of membranes are central to their functions. Membranes are essential for many fundamental cellular processes including ion balance, energy generation, and secretion. In cell division, membrane dynamics are particularly important, where they act to segregate the contents of the cellular progeny.

The process of cell division differs among cells. Most commonly, animal cells divide through a mechanism requiring the assembly of an actin-based contractile ring at the division site (reviewed in Green *et al.* 2012). This actomyosin ring contracts and matures, ultimately leading to scission of the membrane necks mediated by the ESCRTIII (endosomal sorting complex required for transport III) complex. However, other variations of cytokinesis occur: cellularization during early *Drosophila* embryogenesis, which requires the growth of membranes around the nuclei before the contractile event (Lee and Harris 2014) and cell division in plants, which requires the secretion of vesicles to the division plane to form the phragmoplast, which will eventually separate the two daughter cells (reviewed in Jürgens 2005). Actin is not always involved in cytokinesis; although prokaryotic cells have actin-like filaments (reviewed in Carballido-López 2006), these filaments are not used for cytokinesis (Pollard and Wu 2010). Similarly, cytokinesis in *Trypanosoma brucei* (a bikont eukaryote) does not require actin but seems to utilize microtubules (Wheeler *et al.* 2013). In the budding yeast *Saccharomyces cerevisiae*, an actin-based contractile ring plays a role in cytokinesis in vegetatively growing cells (Bi *et al.* 1998; Balasubramanian *et al.* 2004). However, actin does not appear to be involved in the closure of the prospore membrane that grows around the meiotic product during sporulation (Taxis *et al.* 2006).

Sporulation in *S. cerevisiae* occurs as diploid cells experience nutritional stress. The diploid mother cell undergoes meiosis and spore formation, creating four haploid spores, the yeast equivalent of gametes (Neiman 2011). Haploid

doi: 10.1534/genetics.115.183939
Manuscript received October 20, 2015; accepted for publication May 9, 2016; published Early Online May 11, 2016.
Supplemental material is available online at www.genetics.org/lookup/suppl/doi:10.1534/genetics.115.183939/-/DC1.
[1]Present address: Department of Surgery, Beth Israel Deaconess Medical Center, Boston, MA 02215.
[2]Present address: Merck, 33 Avenue Louis Pasteur, Boston, MA 02115.
[3]Corresponding author: Department of Biology, University of Massachusetts, 100 Morrissey Blvd., Boston, MA 02125. E-mail: linda.huang@umb.edu

nuclei formed during meiosis are encapsulated in a double lipid bilayer membrane called the prospore membrane (PSM). The PSM forms *de novo* after meiosis II (Neiman 1998) and ultimately surrounds each of the haploid nuclei. These PSMs must also capture the necessary cytosolic components, including some organelles, which are needed for the newly forming spore. At the appropriate time, the PSM will close; this closure is a cytokinetic event that creates the four spores within the mother cell. The PSM will be used as the template for the construction of the spore wall, and ultimately becomes the plasma membrane for the newly formed spore (Coluccio *et al.* 2004; Diamond *et al.* 2009).

Growth of the PSM initiates at the spindle pole body (SBP), the yeast equivalent of the centrosome, through the fusion of post-Golgi vesicles (Moens 1971; Neiman 1998; Knop and Strasser 2000). As the PSM grows, it is first shaped like a small horseshoe that then elongates to capture the nucleus and some cytoplasmic content (Diamond *et al.* 2009). As the PSM closes, it takes on a rounded shape (Diamond *et al.* 2009).

The leading edge protein complex (LEP), composed of Don1, Ady3, Irc10, and Ssp1, is found at the growing end of the PSM and is required for proper growth and closure of the PSM (Knop and Strasser 2000; Moreno-Borchart *et al.* 2001; Nickas and Neiman 2002; Lam *et al.* 2014). Ssp1 is the most critical component of the LEP, required for the leading edge localization of the other LEP members (Nag *et al.* 1997; Moreno-Borchart *et al.* 2001). The removal and degradation of Ssp1 occurs at the time of PSM closure (Maier *et al.* 2007).

Degradation of Ssp1 is mediated by *AMA1*, a meiosis-specific activator of the anaphase promoting complex (APC/C), although a direct role for Ama1 in targeting Ssp1 for destruction has not been demonstrated (Cooper *et al.* 2000; Diamond *et al.* 2009; Tan *et al.* 2010). The APC/C is an E3 ubiquitin ligase made up of multiple proteins, which requires an activator for proper substrate selection (reviewed in McLean *et al.* 2011). During meiosis, the Cdc20 mitotic activator is required along with Ama1 to regulate APC/C activity (Pesin and Orr-Weaver 2008; Cooper and Strich 2011). APC^{AMA1} has multiple substrates, including Clb1, Pds1, and Ndd1 (Cooper *et al.* 2000; Oelschlaegel *et al.* 2005; Penkner *et al.* 2005; Okaz *et al.* 2012). *AMA1* is needed during meiotic prophase, as *ama1*Δ cells form a MI spindle early, but ultimately form MII spindles at the proper time (Cooper *et al.* 2000; Okaz *et al.* 2012).

The main phenotype seen in *ama1*Δ mutants is during spore morphogenesis (Coluccio *et al.* 2004; Diamond *et al.* 2009). *AMA1* is required for proper closure of the prospore membrane, and *ama1*Δ mutants have stabilized Ssp1 at the leading edge of the PSM (Diamond *et al.* 2009). Cells lacking *AMA1* have normal membrane initiation, but have an extended elongation phase with a partial defect in closure of the prospore membrane. Approximately 30% of *ama1*Δ cells form rounded and closed prospore membranes. Because the closure defect in *ama1*Δ was incomplete, it has been proposed that there may be an *AMA1*-independent pathway acting during prospore membrane closure (Diamond *et al.* 2009).

SPS1 encodes a GCKIII kinase (Slubowski *et al.* 2014) required for sporulation (Friesen *et al.* 1994). Since its discovery and initial characterization (Percival-Smith and Segall 1986; Friesen *et al.* 1994), *SPS1* has been associated with a broad set of functions during sporulation, including histone phosphorylation, spore wall enzyme trafficking, and Gas1 internalization (Iwamoto *et al.* 2005; Krishnamoorthy *et al.* 2006; Rolli *et al.* 2011).

In this study, we identify *SPO77* as a high-copy suppressor of *SPS1*. We find a new role for *SPS1* and *SPO77* in PSM development and find that they act together in this role. Cells lacking *SPS1* and *SPO77* display hyperelongated PSMs that close less frequently than in wild-type (WT) cells and do not remove and degrade the leading edge protein complex in a timely fashion. Finally, we examine the relationship of *SPS1* and *SPO77* with the previously described *AMA1*-dependent pathway for PSM closure (Diamond *et al.* 2009) and find that they function in parallel with *AMA1*. The results collectively suggest that the *SPS1* pathway is involved in PSM closure and that it functions in parallel with the previously described *AMA1*-dependent pathway for PSM closure (Diamond *et al.* 2009).

Materials and Methods

Strains, yeast growth, and induction media

All strains in this study are in the SK1 background (Kane and Roth 1974), and listed in Supplemental Material, Table S1 and Table S2. Standard genetic methods were used to create strains unless otherwise noted (Rose and Fink 1990). Epitope-tagged strains and gene knockout strains were created using PCR-mediated integration as previously described (Longtine *et al.* 1998; Lee *et al.* 2013). Primers and plasmids used in this study are listed in Table S3 and Table S4.

Cells were grown in standard yeast media and sporulated in a synchronous manner in liquid media, as previously described (Huang *et al.* 2005). Unless otherwise noted, all liquid cultures were grown within an Erlenmeyer flask in a shaking incubator at 30°. Cells to be sporulated were first grown to saturation in YPD overnight at 30° and then transferred to YPA and grown to ~1.3 OD_{600}/ml overnight. These cells were then harvested, washed in double-distilled H_2O (ddH_2O), and resuspended in 1% potassium acetate at 2.0 OD_{600}/ml. Sporulation of cells containing plasmids was the same as above except instead of YPD, cells were grown in synthetic dextrose (SD) media, lacking the appropriate nutrient for selection.

Sporulation efficiency counts

Cells that were to be counted for sporulation efficiency were sporulated as above. Cultures in triplicate were incubated at 30° for 24 and 48 hr, as indicated. Aliquots were withdrawn and placed on a slide and examined using a bright-field microscope. At least 200 cells per culture (done in triplicate) for

a total of at least 600 cells per strain were counted for refractile spores or refractile spore-like structures. All cells containing *HTB2*:mCherry were assessed for meiotic efficiency at 9 hr postinduction.

Ninety-six-well plasmid isolation

Library plasmids were isolated from glycerol bacterial stocks by a STET (sodium chloride, Tris-HCl, EDTA, Triton)-BSA boiling miniprep protocol (Holmes and Quigley 1981) adapted for the 96-well format. Bacterial cells containing library plasmids were thawed from glycerol stocks onto LB plates containing kanamycin. After incubation overnight at 37°, colonies were then pinned into deep-well (2.2 ml) 96-well plates containing Terrific Broth plus kanamycin liquid media and grown overnight at 37° to saturation. All spin steps were conducted at 4° unless otherwise noted. These cultures were then spun down at 5000 × *g*, and the pellet was resuspended in 195 μl of STET-Lyso-BSA lysis solution. This was transferred into a 96-well PCR plate, sealed with a foil plate sealer, and heated to 99° for 1 min, then cooled to 4° for 1 min in a thermocycler. Resulting lysates were then spun at 5000 × *g* for 20–30 min as needed to achieve a suitably tight pellet. Once pelleted, 100 μl of the supernatant was removed and transferred to a round-bottomed 96-well storage plate and mixed with 100 μl of IPP (75% isopropanol: 25% 10 M ammonium acetate) solution to precipitate the DNA, and spun to pellet the DNA. The pellet was then washed with 150 μl of 80% ethanol and resuspended in 45 μl of 10 mM pH 8.0 Tris. Plates were then sealed and stored at −20° for later use.

Ninety-six-well yeast plasmid transformation

Library plasmids were transformed into yeast using a transformation protocol (Gietz and Schiestl 2007) adapted for a 96-well format and optimized for the SK1 strain background. The parent yeast strain (LH1060) was grown overnight in a 2800-ml Erlenmeyer flask containing 250 ml of SD −Ura liquid media to a concentration of ∼0.9 ± 0.1 OD_{600}. Then 5.0×10^9 cells were harvested, washed with 0.1 M lithium acetate (LiOAc), and resuspended in 1 ml 0.1 M LiOAc. A total of 1.1 ml of the pooled cells were mixed with 825 μl of 1 M lithium acetate and 2.2 ml of salmon sperm single-stranded DNA, per 96-well plate to be transformed. A total of 38 μl of this cell transformation mixture was transferred to each well in a round-bottomed 96-well plate with 15 μl of plasmid DNA from the library and mixed with 100 μl of 50% PEG. The plate was then sealed and transferred to a 42° shaking incubator to heat shock for 5 hr. After heat shock, cells were pelleted, resuspended in 14 μl of sterile water, and transferred in two ∼9-μl duplicates on a SD −Ura −Leu plate. Plates were then incubated face up for 2–3 days until significant colony growth was observed and then pinned onto a fresh SD −Ura −Leu plate. Resulting duplicate patches were pinned into 150 μl of SD −Ura −Leu liquid media in round-bottomed 96-well plates and grown overnight. The resulting cultures had 60 μl of 40% glycerol added, sealed with foil plate sealers, and frozen in the −80° freezer. Any plasmids that failed to transform by this high-throughput method were then transformed using standard lithium acetate transformation.

Screen and plasmid construction

C-terminal tagging of *SPS1* with three tandem copies of GFP resulted in a hypomorphic allele, which we call *sps1**. *sps1** was mated with a strain containing *HTB2* tagged with mCherry (LH902; Parodi *et al.* 2012) for tracking meiosis, and then transformed with pRS426-G20 (Nakanishi *et al.* 2004) to allow for the visualization of PSM dynamics, which resulted in strain LH1060. This strain was grown, aliquoted into 17 96-well plates, and transformed with the 1588 plasmids of the Minimal Tiled Library (Jones *et al.* 2008) high-copy overexpression plasmid library using methods described above. All subsequent steps were carried out in 96-well plates unless otherwise noted. The resulting strains were then grown in liquid SD −Leu −Ura media to saturation, transferred to YPA overnight, spun down, and resuspended in 750 μl of 1% potassium acetate along with a single 2-mm glass bead to increase aeration. This suspension was placed in a 30° shaking incubator for 24–48 hr before screening.

Cells were screened using a Zeiss Axioskop 2 microscope using DIC and a ×100 1.45 numerical aperture (N.A.) lens. Cells were screened for the production of refractile spores. If necessary, plates were resporulated until satisfactory meiotic performance was achieved for all wells. Any plasmid that appeared to behave as a high-copy suppressor (by creating more refractile spores) was rescreened by retransforming the library plasmid into yeast and sporulating again in Erlenmeyer flasks using conventional high-efficiency methods. These cultures were then reassessed for increased refractile structure formation. Plasmids that were deemed to increase the formation of refractile structures using these methods were considered to be suppressors of *sps1**.

Since each plasmid contained multiple genes, each gene was cloned individually into pRS423, a high-copy vector (Sikorski and Hieter 1989). Fragments of the pGP564 plasmids from the Minimal Tiled Library that suppressed *sps1** were amplified using PCR that added either *Xho*I and *Cla*I or *Xho*I and *Sac*I sites, depending on the sequence of the insert. To construct pRS423-*SPO77*, template pGP564-YGPM4k18 was used in conjunction with primers OLH1253 and OLH1254. To construct pRS423-*SPS1*, template pGP564-YGPM1j19 was used in conjunction with primers OLH1332 and OLH1333. To construct pRS423-*STP2*, template YGPM30n09 was used in conjunction with primers OLH1241 and OLH1242. *SPO77* and *SPS1* inserts were tested by complementation of their respective genomic null mutants. Each of these plasmids was then transformed back into LH1060, sporulated using standard methods, and reassessed for refractile structure formation indicative of spore formation.

The plasmid pCS232 was created by PCR amplification of GFP^{Envy} from pFA6a-link-Envy-SpHIS5 (Slubowski *et al.* 2015) using primers OLH1493 and OLH1494, which

incorporated *Eco*RI and *Hin*dIII restriction sites flanking GFP^{Envy}. pRS316-pr*SPS1*-SBP-*SPS1* (Slubowski *et al.* 2015) and the GFP^{Envy} PCR product were cut with *Eco*RI and *Hin*dIII, removing the streptavidin binding peptide (SBP) epitope and producing ligation-compatible overlaps, which allowed the creation of pRS316-pr*SPS1*-Envy-*SPS1*. pRS316-pr*SPS1*-Envy-*SPS1* and empty pRS424 vector were then digested with *Sac*I and *Kpn*I and the entire pr*SPS1*-Envy-*SPS1* insert was ligated into the pRS424 backbone, creating pCS232 (pRS424-pr*SPS1*-Envy-*SPS1*).

Fluorescence microscopy

All fluorescent images were visualized using a Zeiss Axioskop 2 fluorescent microscope using a ×100 N.A. 1.45 lens. Images were captured using a Hammamatsu OrcaER CCD camera run by the Open Lab imaging software. All cells were imaged under live conditions unless otherwise noted. Cells were optically sectioned in the *Z*-plane for each channel. *Z*-section images were adjusted for equivalent brightness and contrast and merged.

PSM time-lapse videos and projections

All videos and three-dimensional projections of sporulating cells were done on a Zeiss LSM 510 confocal microscope and captured with Zeiss LSM 510 software. Time-lapse videos were taken using a CellASIC microfluidics chamber and Millipore Y-04D plates. Cells were captured in the visualization chamber between 4 and 5 hr after induction in sporulation media (using standard sporulation methods described above). While in the chamber, additional sporulation media was perfused at 6 psi for the duration of imaging. Images were taken every 2 min for the duration of the video with a pinhole aperture of 540 and 512 × 512 resolution and scan time of 7.6 μs/pixel. Three dimensional projections were imaged in the same manner as time-lapse images, except a *Z*-stack was taken of a cell and the resulting *Z*-stacks were then projected into a three-dimensional view using the LSM 510 software for a ±45° view at 6° intervals.

PSM size and nuclear capture quantification

All PSM size measurements were made as previously described (Parodi *et al.* 2012) using ImageJ software (Schneider *et al.* 2012) on images collected as described above. Briefly, an image stack of optical sections was taken of individual postmeiotic cells and PSM size was determined by measurement of the maximal projection of each rounded PSM.

Nuclear capture was scored on live postmeiotic cells with rounded PSMs and merged optical sections of PSM and Htb2-mCherry signal were used to assess whether each of the nuclei were fully captured by the closed PSM. The number of captured nuclei per ascus was quantified as in Parodi *et al.* 2012.

Western blotting

Cells were collected at the indicated times and prepared using the TCA method (Philips and Herskowitz 1998), which involves first lysing cells in a lysis buffer (1.85 N NaOH and 10% v/v betamercaptolethanol) followed by precipitation of proteins with 50% (v/v) trichloroacetic acid (TCA). TCA-precipitated protein lysates were then washed with ice-cold acetone and resuspended in 1× sample buffer neturalized with 5 μl of 1 M Tris base before boiling for 5 min. Protein lysates were separated on SDS-PAGE gels. Protein was transferred onto Immobilon LF-PVDF membrane, blocked, and incubated overnight with the appropriate primary antibodies. Sps1-GFP (*sps1**) and sf-GFP were detected using JL-8 anti-GFP antibodies (Takara/Clontech) at 1:1000; Ssp1-myc was detected using 9E10 anti-myc antibodies (Covance) at 1:1000; Pgk1 was detected by using 22C5D8 anti-Pgk1 (Life Technologies) (1:1000); Tub1 was detected using monoclonal mouse 12G10 anti-Tub1 antibody at 1:1000 concentration (Developmental Studies Hybridoma Bank). Fluorescent infrared-dye-conjugated anti-mouse secondary antibodies were used at 1:20,000 (LI-COR). All membranes were imaged using an Odyssey Infrared Imaging System (LI-COR).

Quantification of protein levels

Proteins were quantified using the Image Studio v3.1 software from LI-COR. Bands from Western blots were quantified using four-pixel top–bottom median background correction, and the total signal value was used for protein level comparisons. For looking at Ssp1 levels, blots were quantified by normalizing the Ssp1-13x-myc signal to the Pgk1 signal for the lane, then normalizing the resulting Ssp1/Pgk1 ratios to the ratio of that blot, to show the relative Ssp1 expression pattern in each genetic background.

Protein stability assay

Protein stability was assayed using the translational inhibitor cycloheximide. Cycloheximide was added to cultures 8 hr after transfer to sporulation media. Aliquots were subsequently withdrawn every 15 min after the addition of cycloheximide and pelleted. The samples were then processed by TCA precipitation and SDS-PAGE analysis, as described above. Three biological replicates for each strain were analyzed, and Ssp1-myc was normalized to the long-lived Tub1 levels. An ANCOVA test was used to calculate the significance of the difference in Ssp1 stability seen between WT and *sps1*Δ.

Phos-tag analysis

Phos-Tag gels were made using Phos-tag acrylamide AAL-107 (WACO) at a final concentration of 31.4 μM Phos-tag and 50.6 μM $MnCl_2$ in an otherwise standard SDS-polyacrylamide gel, as in Whinston *et al.* (2013). Samples were prepared as above and run at 80 V at 4° before being transferred and imaged, as above.

Immunoprecipitation

To co-immunoprecipitate Sps1 and Ssp1, cultures of cells were sporulated while meiosis was monitored, to ensure synchronous sporulations both within and between cultures. When sfGFP-Sps1 fluorescence was visible in the majority

of cells, cells (120 OD_{600}) were harvested and flash frozen in liquid nitrogen, along with parallel samples (three OD_{600}) for Western analysis, as described above. Samples for co-immunoprecipitation were taken and lysed in IP buffer (16 mM HEPES, 1.2 mM $MgCl_2$, 330 mM NaCl, 0.8% v/v NP40, 0.08 mM EDTA) with phosphatase and protease inhibitors, as previously described (Slubowski *et al.* 2014). Resulting cell lysates were precleared using blocked agarose beads (Chromotek) for 1 hr before the supernatant was removed and placed on GFP-trap-conjugated agarose beads for 2 hr at 4° (Chromotek). Beads were washed four times in IP buffer, resuspended in 2× sample buffer, and boiled for 5 min. Samples were analyzed on a 10% SDS-PAGE gel, as described above.

Data and reagent availability

Strains and plasmids are available upon request. The authors state that all data necessary for confirming the conclusions presented in the article are represented fully within the article.

Results

Screening for high-copy suppressors of SPS1

To identify genes that interact with *SPS1*, we screened a tiled 2μ library of 1588 plasmids covering ~98% of the genome (Jones *et al.* 2008) for their ability to suppress *sps1**. *sps1** is a C-terminal Sps1-3 × GFP fusion protein that does not complement *sps1*Δ. Cells homozygous for *sps1** form 6.2% refractile spores, which is intermediate between wild type (86.2%) and the *sps1Δ* null allele (1.8%), consistent with *sps1** acting as a hypomorphic allele (Figure 1A). *sps1** does not act in a dominant negative fashion, as the sporulation efficiency of *SPS1/sps1** is similar to wild type (Figure 1A). Consistent with *sps1** being a hypomorphic allele (and not a protein null), the protein encoded by *sps1** can be detected on an immunoblot (Figure S1). We chose to suppress a hypomorphic allele to facilitate the isolation of a broader range of suppressors than might be obtained using a null.

Plasmids containing the library were transformed into *sps1**, sporulated in 96-well plates, and visually screened for the formation of refractile spores (Figure 1B). As sporulation is less efficient in 96-well plates, candidate strains yielding >10% refractile spores were reassessed for spore formation using conventional high-efficiency liquid sporulation conditions. Four plasmids from the library reproducibly suppressed the *sps1** phenotype: YGPM4k18, YGPM1j19, YGPM18n12, and YGPM30n09 (Figure 1C). Two plasmids, YGPM1j19 and YGPM18n12, contained *SPS1*, while YGPM4k18 and YGPM30n09 harbored candidate suppressors. Each individual gene contained within YGPM4k18 and YGPM30n09 was subcloned into the high-copy vector pRS423 (Sikorski and Hieter 1989). This analysis revealed that the suppression observed by YGPM4k18 and YGPM30n09 could be accounted for by *SPO77* and *STP2*, respectively (Figure 1D).

Previous studies demonstrated that null alleles of *SPO77* do not form refractile spores (Rabitsch *et al.* 2001; Coluccio *et al.* 2004). *SPO77* encodes a protein with no known conserved functional domains and appears specific to fungi. We confirmed that *spo77*Δ mutants are defective in forming refractile spores, but detected no defects in refractile spore formation in *stp2*Δ mutants (Figure 2A).

STP2 encodes a transcription factor that controls the expression of genes responsible for the import of amino acids across the plasma membrane (de Boer *et al.* 2000). *STP2* has a paralog, *STP1*, that also plays a redundant role in amino acid transport (de Boer *et al.* 2000); *STP1* overexpression (plasmids YGPM10d14 and YGPM17l13) did not suppress *sps1**. As *STP2* had no obvious sporulation defect, we chose to focus on *SPO77*.

SPO77 genetically interacts with SPS1

To further examine the relationship between *SPS1* and *SPO77*, we examined spore formation in the *spo77*Δ*sps1*Δ double mutant. Consistent with a role in the same (rather than parallel) pathways, *spo77*Δ*sps1*Δ mutants formed spores at a similar level to either single mutant (Figure 2A). In contrast to its ability to suppress the *sps1** hypomorph, *SPO77* overexpression failed to suppress the *sps1*Δ null, (Figure 2B), suggesting that some level of *SPS1* activity is required for *SPO77* to suppress *SPS1*. *SPS1* overexpression also failed to suppress the *spo77*Δ null (Figure 2C).

SPS1 and SPO77 play a role in PSM development

As refractile spore formation is the terminal phenotype of a complex process, we reasoned we could more precisely understand the roles of *SPS1* and *SPO77* in spore morphogenesis by assaying earlier events. Thus, we chose to examine the formation of the PSMs, an early event during spore formation that occurs as cells are undergoing meiosis II (Neiman 2011) using a PSM marker (pRS426-G20, which is a GFP fusion to residues 51–91 of Spo20) (Nakanishi *et al.* 2004). PSMs in WT cells underwent development as previously reported, with PSMs initiating at the spindle poles of cells in meiosis II, elongating around the meiotic nucleus, and rounding up as they close to form the four individual prospores as meiosis II is completed (Figure 3A) (Diamond *et al.* 2009).

Both *sps1*Δ and *spo77*Δ mutants had aberrant PSM development, exhibiting hyperelongated and often convoluted PSMs at the latest stages of PSM development that give rise to rounded, but smaller than WT PSMs (Figure 3, A–C and Figure 4A; projections shown in File S1, File S2, File S3, File S4, File S5, and File S6). We confirmed that these hyperelongated PSMs lead directly to the small, round PSM phenotype, by following single cells using time-lapse microscopy (File S7, File S8, File S9; legends for movies File S10). PSM perimeter was quantified after rounding, with WT cells forming PSMs with a perimeter of 7.4 ± 0.9 μm, while both *sps1*Δ and *spo77*Δ form PSMs with perimeters of 5.8 ± 1.3 μm (Figure 4B).

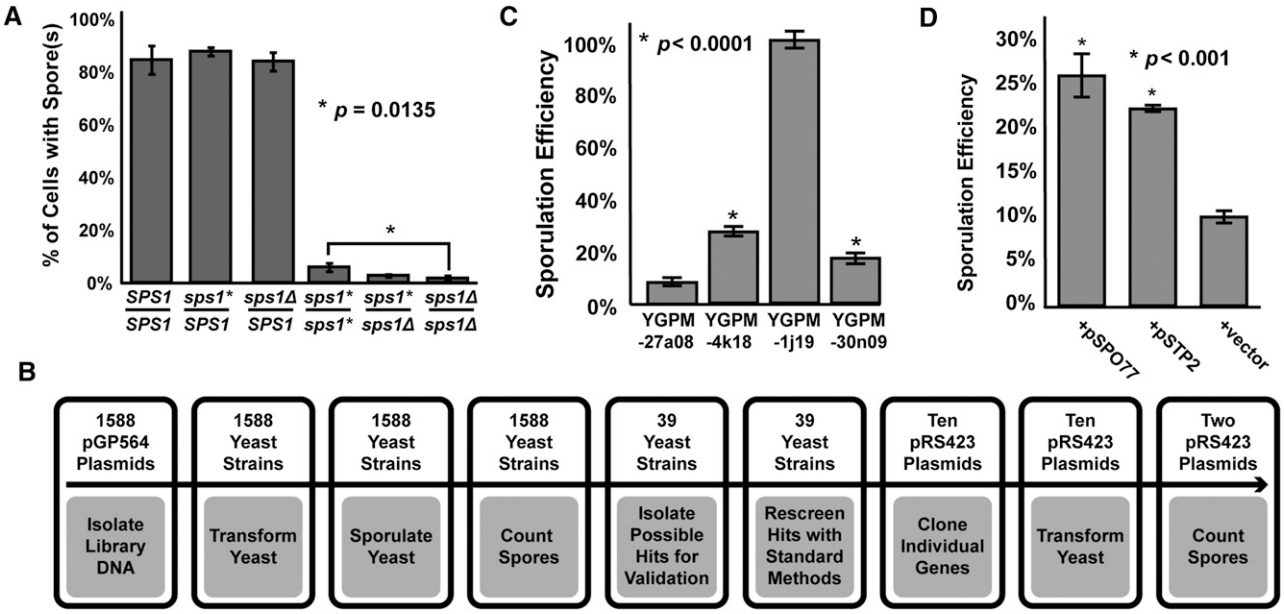

Figure 1 *STP2* and *SPO77* are high-copy suppressors of *sps1*. (A) *sps1** is a hypomorphic allele of *SPS1*. Cells of the indicated genotypes were sporulated and assessed for refractile spore formation 24 hr postsporulation induction (strains from left to right LH177, LH1020, LH1017, LH1019, LH1018, and LH872). For each strain, at least 200 cells were counted from triplicate cultures. (B) A schematic of the pipeline used for a high-copy suppression screen of the hypomorphic allele *sps1**. Numbers at the top describe the number of hits carried on through the step in the gray box found below. (C) Plasmids isolated from the library were retested under conventional high-efficiency conditions and assessed for refractile spore formation and normalized to the level of suppression of *sps1** seen with YGPM1j19, which contains *SPS1* (strains from left to right LH1037, LH1035, LH1034, and LH1036). The *sps1** strain harboring the control plasmid (YGPM27a08), the 2μ-*SPS1*-containing plasmid (YGPM1j19), the 2μ-*SPO77*-containing plasmid (YGPM4k18), and the 2μ-*STP2*-containing plasmid (YGPM30n09) sporulated at 3, 45, 12, and 8%, respectively. (D) Genes and their native promoters were cloned from the two library plasmids that showed suppression of *sps1** into pRS423, assessed for suppression of *sps1**, and normalized to the level of suppression seen with YGPM1j19, which contains *SPS1* (strains from left to right LH1038, LH1039, and LH1040). All error bars in B–D indicate standard deviation; *P*-values were calculated using an unpaired *t*-test.

We also see a slight decrease in the ability of the PSMs to properly capture nuclei in the mutant backgrounds. Nuclear capture was quantified at two time points: early in PSM development, just before or immediately after elongation began and again after closure. Early in PSM development there was nearly 100% nuclear envelopment in all strains examined. However, we saw a modest (~10%) decrease compared to WT in nuclear capture for *sps1*Δ and *spo77*Δ cells that had rounded PSMs (Figure 4C). This suggests that PSMs initially grow around the nuclei but that the nuclei sometimes escape capture before PSM closure.

The *sps1*Δ*spo77*Δ double mutant is indistinguishable from either single mutant in all phenotypes examined, including PSM morphology (Figure 4D), PSM size (Figure 4B), and nuclear capture (Figure 4C). Thus, both *SPS1* and *SPO77* exert similar effects on PSM development and exhibit genetic interactions consistent with acting in the same, rather than parallel, pathways.

Sps1 has a dynamic localization during sporulation

We previously reported that a superfolder-GFP-Sps1 (sfGFP-Sps1) fusion protein localizes to the nucleus and the cytoplasm during sporulation (Slubowski *et al.* 2014). Due to the observed PSM defect in *sps1*Δ cells, we reexamined sfGFP-Sps1 localization and detected a dim, transient localization at the PSM (Figure S2). sfGFP folds and matures quickly but photobleaches rapidly (Lee *et al.* 2013; Slubowski *et al.* 2015). The PSM localization of sfGFP-Sps1 fades to undetectable levels within 3 sec of epifluorescent illumination, making it difficult to observe.

To better capture the localization of Sps1, we fused Sps1 to the GFP variant Envy, which is brighter and more photostable than sfGFP (Slubowski *et al.* 2015). Envy-Sps1 was expressed under the control of the *SPS1* promoter from a high-copy plasmid in a strain lacking endogenous *SPS1*, alongside the blue fluorescent PSM marker Spo20$^{51-91}$-mTagBFP (Lin *et al.* 2013) (Figure 5). Envy-Sps1 complements *sps1*Δ, as *sps1*Δ cells with this plasmid form refractile spores. We observed colocalization between Envy-Sps1 and the PSM marker during the elongation phase (Figure 5). As the PSMs round up, Envy-Sps1 accumulates in the nucleus and the cytosol, as previously reported for sfGFP-Sps1. Thus, Sps1 can localize to the PSM during PSM development, and concentrates in the nucleus as the PSMs close.

SPS1 and SPO77 are required for the removal of the LEP

The LEP coat is a proteinaceous structure found at the leading edge of the growing PSM. The LEP is thought to provide structural support and directional guidance for

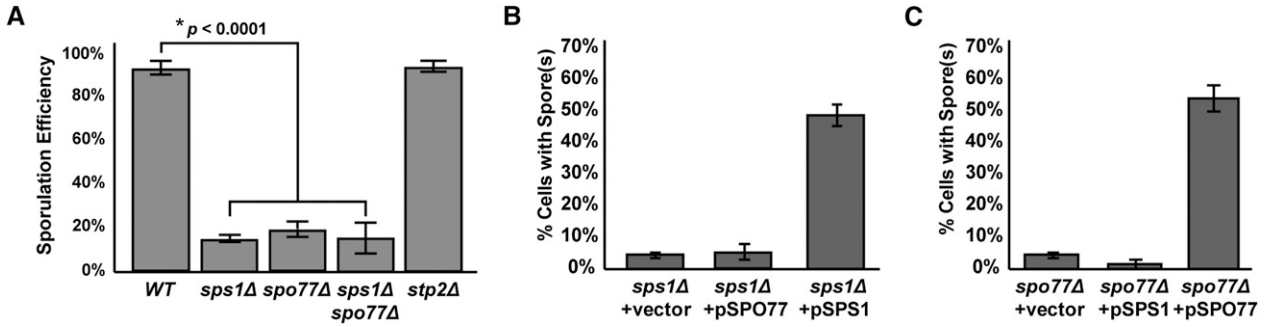

Figure 2 *SPS1* and *SPO77* interact. (A) *WT*, *sps1*, *spo77*, *sps1spo77*, and *stp2* knockout strains (LH902, LH976, LH1010, LH1012, and LH1016, respectively) were assessed for refractile spore formation. All experiments were counted at 24 hr postinduction. (B) *sps1*Δ null strains sporulated with *SPO77* on a high-copy plasmid (from left to right LH1041, LH1042, and LH1043). (C) *spo77*Δ null strains were sporulated with *SPS1* on a high-copy plasmid (from left to right LH1044, LH1046, and LH1045). For the experiments in A–C, at least 200 cells were counted from each culture and all cultures were grown and sporulated in triplicate. All error bars in A–C indicate standard deviation; *P*-values were calculated using an unpaired *t*-test.

the PSM, and is removed when the PSM closes (Maier *et al.* 2007; Diamond *et al.* 2009). Because the PSMs of *sps1*Δ and *spo77*Δ mutants are irregularly shaped late in their development, we examined whether the LEP was disturbed by assessing the localization of the LEP coat member Don1 (Knop and Strasser 2000). Don1 was tagged with GFP (Huang *et al.* 2005) and its localization was examined in WT, *sps1*Δ, and *spo77*Δ cells.

We observe Don-GFP localization to the leading edge of the PSM in WT cells during PSM elongation (Figure 6A, left), as previously observed (Knop and Strasser 2000; Diamond *et al.* 2009). Similarly, *sps1*Δ and *spo77*Δ cells have Don1-GFP at the leading edge of elongated PSMs as well as in hyperelongated PSMs (Figure 6, B and C, both left). When WT cells have rounded PSMs, Don1-GFP is removed from the PSM and becomes faint and diffuse within the newly formed PSM (Figure 6A, right) (Maier *et al.* 2007; Diamond *et al.* 2009). In contrast, in both *sps1*Δ and *spo77*Δ mutant strains, Don1-GFP remains bright and generally localized to puncta associated with the PSM (Figure 6, B and C, both right). The Don1-GFP puncta are not properly removed from closed prospore membranes in *sps1*Δ and *spo77*Δ cells compared to WT (Table 1; *P*-value <0.0001). These results suggest that *SPS1* and *SPO77* are not required for the correct initial localization of the LEP, but are required for proper LEP disassembly.

The LEP is removed as PSMs close, and previous work has shown that *AMA1* regulates PSM closure and is required for proper LEP removal (Maier *et al.* 2007; Diamond *et al.* 2009). We see that *ama1*Δ cells make rounded PSMs that retain bright Don1-GFP puncta (Figure 6D, right) as previously shown (Diamond *et al.* 2009; Park *et al.* 2013), at a frequency similar to what was observed in the *sps1*Δ and *spo77*Δ mutants (Table 1; *P*-value <0.0001). We also observe hyperelongated PSMs in *ama1Δ* cells (Figure 6D, left), consistent with previous reports (Diamond *et al.* 2009). Given the similarity of the *sps1Δ* and *spo77Δ* phenotypes to the *ama1Δ* phenotype, we hypothesized that *SPS1* and *SPO77* may have a role in PSM closure similar to *AMA1*.

SPS1 and SPO77 are required for PSM closure independent of AMA1

To test whether *SPS1* and *SPO77* act in the same pathway as *AMA1* to regulate PSM closure, we examined PSM development in double mutants of *sps1*Δ*ama1*Δ and *spo77*Δ*ama1*Δ. As expected, early PSM morphology was relatively normal (Figure 7, A and B). However, as cells approached the time that WT strains would have rounded PSMs and begin showing refractile structures indicative of spore wall development, both double mutants display a hyperelongated PSM morphology similar to that of the *sps1Δ* and *spo77Δ* single mutants (Figure 7, A and B). Unlike in *sps1*Δ, *spo77*Δ, and *ama1*Δ single mutants, the hyperelongated PSMs never develop into round structures in the *sps1*Δ*ama1*Δ and *spo77*Δ*ama1*Δ double mutants. This is true even as late as 12 hr after sporulation induction, when WT cells have completed spore morphogenesis. At late time points, the entire cell cytoplasm of *sps1*Δ *ama1*Δ and *spo77*Δ *ama1*Δ double mutants fills with heavily invaginated PSM material (Figure 7, A and B, yellow arrows), with nearly all nuclei contained within the PSM (Figure 7, A and B, white arrows). Taken together, these data suggest that *sps1*Δ*ama1*Δ and *spo77*Δ*ama1*Δ double mutants can still target nuclei but completely lack the ability to form rounded PSMs. Because the *sps1*Δ*ama1*Δ and *spo77*Δ*ama1*Δ double mutants show sporulation defects more severe than either the *sps1*Δ or *spo77Δ* single mutant, and because the *sps1*Δ*spo77*Δ PSM phenotype is indistinguishable from either single mutant, this suggests that *SPS1* and *SPO77* function in an independent pathway that acts in parallel and is partially redundant with the *AMA1* pathway that regulates PSM closure.

Because the removal of the LEP from the leading edge of the PSM is mediated by *AMA1* and is correlated with PSM closure, we asked whether loss of *SPS1* or *SPO77* exacerbated the previously described *ama1*Δ defect of incomplete removal of LEP material at the time of PSM closure (Diamond *et al.* 2009). Double mutants of both *sps1*Δ*ama1*Δ and *spo77*Δ*ama1*Δ were sporulated and the LEP was visualized using Don1-GFP. Both double mutants

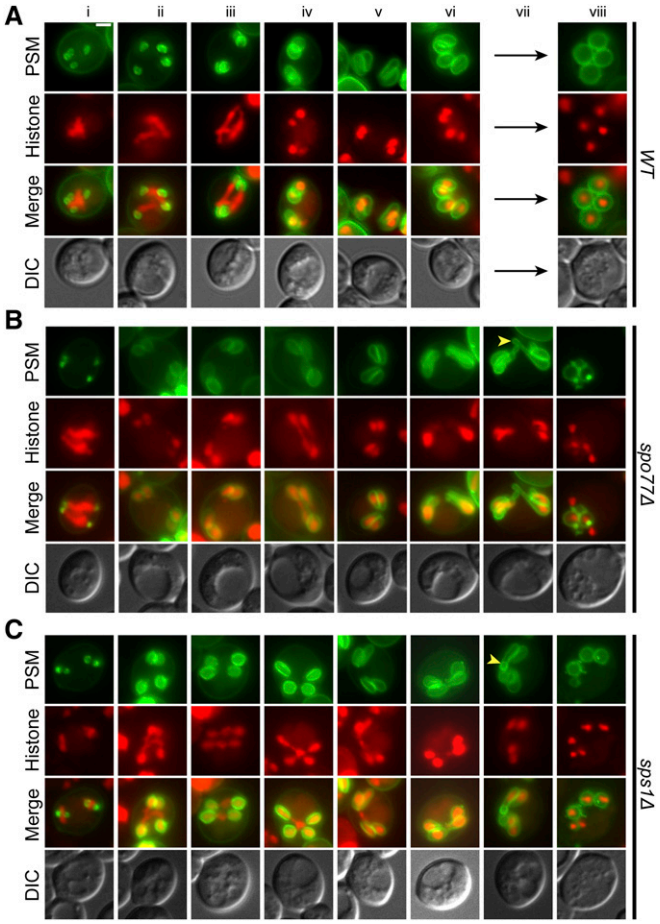

Figure 3 *SPO77* and *SPS1* have similar roles for PSM development during sporulation. PSMs are labeled using a plasmid containing pRS426-G20. Nuclei are labeled using genomically integrated *HTB2*-mCherry. (A) PSMs in WT cells (LH917) at various stages of PSM development. Stages are as follows: (i) pinpoints, (ii) early horseshoe, (iii) mid horseshoe, (iv) early elongation, (v) mid elongation, (vi) late elongation, (vii) extreme elongation (does not occur in WT cells), and (viii) rounded/closed. (B) PSMs in *sps1*Δ cells (LH1047). Yellow arrows highlight aberrant PSM morphology. (C) PSMs in *spo77*Δ cells (LH1049).

showed phenotypes similar to the single mutants (Figure 7, C and D), except that few to no rounded PSMs and no dissociated Don1-GFP foci were observed within a double mutant ascus. Full LEP rings were found as late as 12 hr postinduction (Figure 7, C and D, white arrows). The presence of LEP rings in the double mutants, at times when WT cells have completed spore morphogenesis, is consistent with a complete failure in PSM closure. This result suggests that *SPS1*, *SPO77*, and *AMA1* are required to disassemble and degrade the LEP during the course of PSM development.

Because we saw that the LEP was not properly removed, we asked whether PSM-mediated cytokinesis was affected in these mutants. We first examined PSM initiation to see whether the timing of PSM formation was altered. None of the strains examined had a delay in the initiation of PSM formation (Figure 8A).

Next, as rounding of the PSMs is an indirect measure of closure (Diamond *et al.* 2009), we examined the appearance of rounded PSMs in the single and double mutants of *SPS1*, *SPO77*, and *AMA1*. We saw delays in the formation of rounded PSMs (Figure 8B). *sps1*Δ and *spo77*Δ single mutants and the *sps1*Δ*spo77*Δ double mutant all displayed similar PSM rounding kinetics, with a delay of ~1 hr compared to WT and the formation of fewer rounded PSMs (*sps1*Δ = 73.0%, *spo77*Δ = 67.5%, and *sps1*Δ*spo77*Δ = 69.5%, compared to 96.5% for WT). These results are consistent with *SPS1* and *SPO77* acting in the same pathway.

The single mutant of *ama1*Δ showed a more severe delay in rounded PSM appearance (~2 hr) and even fewer rounded PSMs (31.0%) than the *sps1*Δ and *spo77*Δ single mutants (73.0 and 67.5%, respectively) or the *sps1*Δ*spo77*Δ double mutant (69.5%) (Figure 8B). The *ama1*Δ *sps1*Δ and the *ama1*Δ *spo77*Δ double mutants fail to form rounded PSMs (0% for both strains) (Figure 8B), consistent with *SPO77* and *SPS1* acting in a parallel pathway to *AMA1* in PSM closure.

SPS1 and SPO77 are required for Ssp1 degradation

Previous studies have shown that Ssp1 is removed from the leading edge and degraded when PSMs close (Maier *et al.* 2007), and that *AMA1* is needed for Ssp1 removal (Diamond *et al.* 2009). Because we see Don1 persistence in rounded PSMs in the *sps1*Δ and *spo77*Δ mutants (Table 1), since *SSP1* is required for Don1 localization (Moreno-Borchart *et al.* 2001), and because *SPS1* and *SPO77* act in parallel to *AMA1*, we asked whether *SPS1* and *SPO77* were also required for Ssp1 removal and degradation. We examined Ssp1 degradation by examining the relative protein levels of the fusion protein Ssp1-13x-myc and see that Ssp1 protein levels decrease during sporulation and that Ssp1 is stabilized in *ama1*Δ mutants, as previously described (Figure 8, C and D; Maier *et al.* 2007; Diamond *et al.* 2009). At 14 hr, Ssp1 is also stabilized in the *sps1*Δ and *spo77*Δ mutants, as well as in the *ama1*Δ *sps1*Δ and the *ama1*Δ *spo77*Δ double mutants (Figure 8, C and D). These mutant strains also all show multiple bands of Ssp1 not seen in WT, which are presumably degradation products. For simplicity, our quantitation (Figure 8D) summed all Ssp1 bands. Because we do not know which bands represent functional Ssp1 at the leading edge of the PSM, the stabilization we see may reflect a stabilization of the total pool (which may include nonfunctional Ssp1), and it is possible that the decline in the functional pool is more modest. The increased instability that we see was not due to obvious differences in the rate of sporulation in the different cultures, as these cultures are progressing through meiosis at nearly identical rates (Figure 8E).

Since *SPS1* appears to act in an independent pathway from *AMA1*, we asked whether it normally acts to promote Ssp1 degradation, like *AMA1* (Diamond *et al.* 2009), or acts by inhibiting Ssp1 production. We distinguished between these possibilities by observing the relative length of time extant

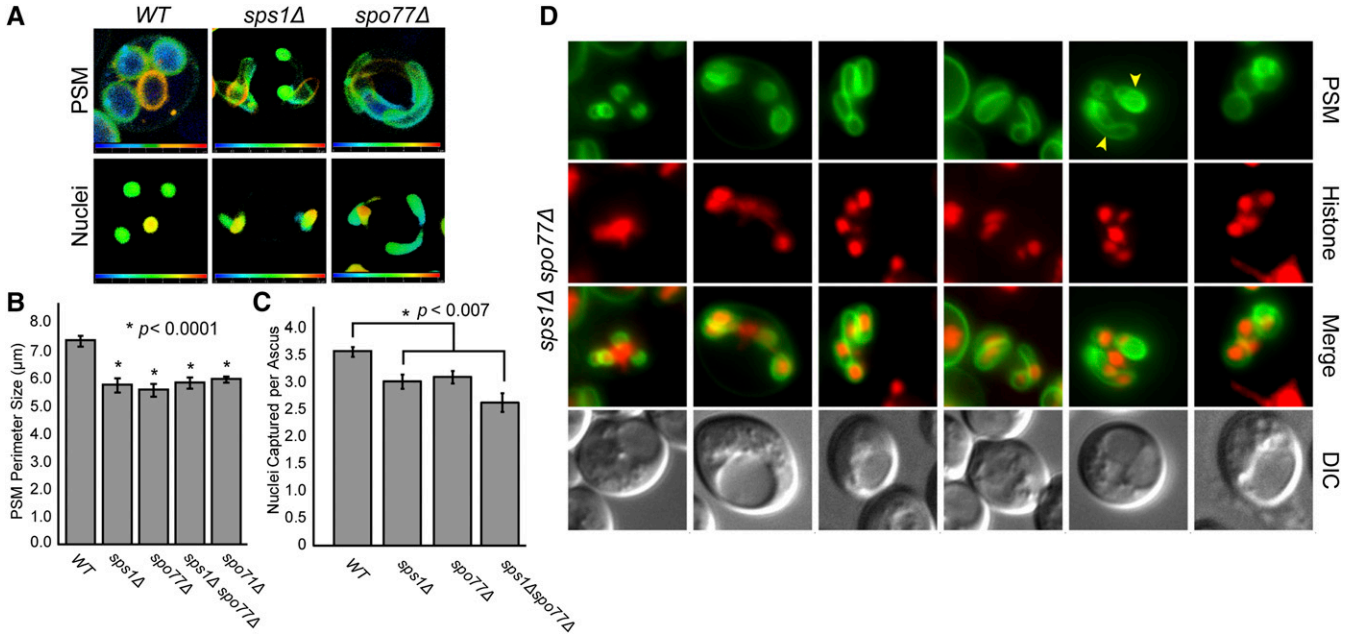

Figure 4 Analysis of PSM development. (A) Live *WT*, *spo77*Δ, and *sps1*Δ cells (LH917, LH1049, and LH1047) were sporulated in a CellASIC microfluidics chamber and imaged via confocal microscopy during late-stage PSM development. Image is a merged *Z*-stack. Depth is indicated by color coding, with blue indicating the most proximal and red indicates the most distal within the *Z*-plane. (B) *SPS1* and *SPO77* are required for proper rounded PSM size. *WT*, *sps1* Δ, *spo77*Δ, and *sps1*Δ *spo77*Δ cells (LH917, LH1047, LH1049, and LH1050) were sporulated. Those cells with four rounded PSMs present were assessed for the perimeter size of the maximum projection of each PSM. For each strain, at least 50 rounded PSMs were analyzed from images taken over at least three cultures. Error bars indicate the SEM; *P*-values were calculated using a paired *t*-test. *spo71*Δ data were included as a positive control for small PSM size. (C) *SPS1* and *SPO77* are required for proper rounded PSM size and nuclear capture. Cells from cultures in A were assessed for nuclear capture in cells with rounded PSM morphology. Error bars indicate SEM; *P*-values were calculated using a paired *t*-test. At least 150 nuclei were counted per strain. (D) PSMs in *sps1*Δ *spo77*Δ cells (LH1050). PSMs are labeled using a plasmid containing GFP-Spo20$^{51–91}$, pRS426-G20. Nuclei are labeled using genomically integrated *HTB2*-mCherry.

Ssp1-13x-myc persists after halting translation using cycloheximide, an inhibitor of translation, to estimate the stability of Ssp1 in WT and the *sps1*Δ mutant. The *sps1*Δ mutant showed increased Ssp1-13x-myc protein stability relative to WT, as normalized to the long-lived Tub1 protein (*P*-value = 0.049; Figure 8F). Taken together, these results suggests that, like *AMA1*, the *SPS1* pathway normally plays a role in promoting the destruction of Ssp1.

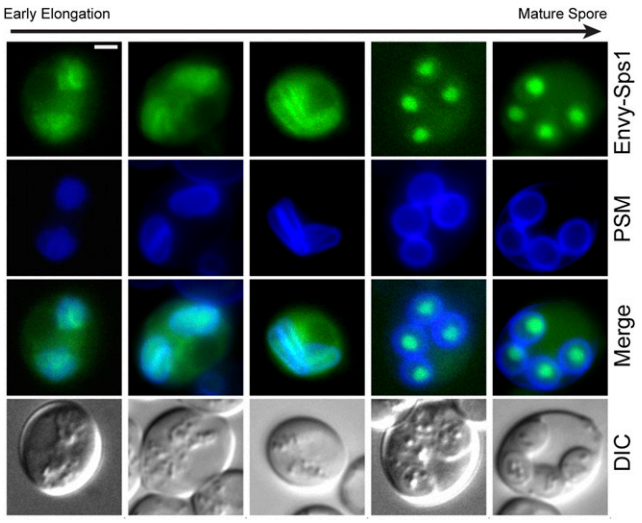

Figure 5 Sps1 is dynamically localized during sporulation. LH1059 cells lacking endogenous *SPS1* that contain Envy-Sps1 on a high-copy plasmid pCS232 (pRS424-prSPS1-Envy-SPS1) and the blue fluorescent PSM marker Spo20$^{51–91}$-mTagBFP were sporulated and observed for colocalization of Envy-Sps1 with the blue PSM marker.

Sps1 interacts with, and is required for the proper phosphorylation of Ssp1

Because Sps1 appeared to be regulating Ssp1 protein levels, we wondered whether this regulation involved a physical interaction. Using a strain where Sps1 and Ssp1 were epitope tagged at the genomic locus, we were able to co-immunoprecipitate sfGFP-Sps1 and Ssp1-13x-myc in sporulating cells (Figure 8G). This result is consistent with Sps1 and Ssp1 being in a complex during sporulation.

Ssp1 has previously been described as a phosphoprotein (Maier *et al.* 2007). Since Sps1 is a serine/threonine kinase and is in complex with Ssp1, we tested whether *SPS1* is required for Ssp1 phosphorylation. We assayed the 10-hr samples from Figure 8C for phosphorylation using a Phos-tag gel, which specifically retards the migration of phosphoproteins through the matrix, allowing resolution of multiple phosphorylation states (Kinoshita *et al.* 2006; Whinston *et al.* 2013). In WT cells, the Ssp1-13x-myc fusion protein migrates as several distinct bands on a Phos-tag gel, consistent with Ssp1 having multiple phosphorylation sites (Figure 8H). In *sps1*Δ and *spo77*Δ

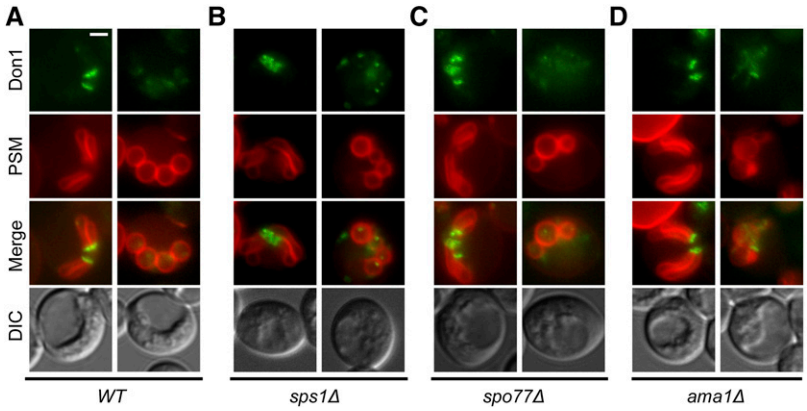

Figure 6 Don1-GFP localization during sporulation in (A) WT (LH1053), (B) *sps1*Δ (LH1054), (C) *spo77*Δ (LH1056), and (D) *ama1*Δ (LH1055). PSMs were visualized using the red fluorescent PSM marker pRS426-R20. For each strain, an image of a cell at late PSM elongation stage (left) and a cell with rounded PSMs (right) are shown. All cells were imaged live and at the same magnification. White bar, 2 μm.

mutants, the most slowly migrating species of Ssp1-13x-myc was missing, although there is also an increase of some presumed degradation products (Figure 8H). However, *ama1*Δ mutants did not show a similar loss of the slowest migrating species of Ssp1-13*x*-myc compared to the *sps1*Δ or *spo77*Δ mutants (Figure 8G). These results suggest that *SPS1* and *SPO77* are required for the proper phosphorylation of Ssp1, and that their effects on Ssp1 modification are distinct from those of *AMA1*. This result is also consistent with *SPS1* and *SPO77* acting independently of *AMA1*.

Discussion

Prior work has demonstrated that closure of the prospore membrane in *S. cerevisiae* depends upon the activator of the meiotic anaphase-promoting complex encoded by *AMA1* (Diamond *et al.* 2009). However, the partial defects observed in *ama1*Δ mutants suggested that another, independent pathway also acts to regulate closure. Here, we find the pathway defined by *SPS1* and *SPO77* act in parallel to *AMA1* to regulate closure, and affects the phosphorylation and stability of Ssp1 (Figure 8, C, D, F, and H). In contrast, *AMA1* is required for the stability of Ssp1 (Figure 8, C and D) but not its phosphorylation (Figure 8H) (Diamond *et al.* 2009).

In our model, we place *SPS1* and *SPO77* together in one pathway, as cells deficient in either *SPS1* or *SPO77* produce hyperelongated prospore membranes, do not properly remove Don1 from the leading edge of the prospore membrane, and have stabilized Ssp1 that is reduced in phosphorylation (Figure 8I). The *sps1*Δ *spo77*Δ double mutant is indistinguishable from either single mutant for prospore membrane size (Figure 4B), nuclear capture (Figure 4C), prospore membrane development (Figure 4D), and prospore membrane closure (Figure 8B), consistent with both genes acting in the same pathway. Interestingly, high-copy *SPO77* can suppress the hypomorphic *sps1** allele, but not the *sps1*Δ null, suggesting that genetic suppression requires at least some *SPS1* activity. Additionally, we could not suppress *spo77*Δ mutants with overexpression of *SPS1*, which may be expected if *SPS1* acted downstream of *SPO77*. It is possible that *SPO77* modulates *SPS1* in some fashion, perhaps acting as a cofactor or scaffold necessary for *SPS1*'s role in Ssp1 degradation. We simply conclude that these two genes act together to promote prospore membrane closure.

Table 1 Don1-GFP persistence in cells with closed PSMs

Strain	% of cells with puncta	*n*	Fisher's exact *P*-value
WT (LH1053)	8.8	103	N/A
sps1Δ (LH1054)	71.7	99	<0.0001
spo77Δ (LH1056)	77.6	85	<0.0001
ama1Δ (LH1055)	88.1	84	<0.0001

We believe that the *SPS1/SPO77* pathway acts in parallel to *AMA1* (Figure 8I), because the *sps1*Δ*ama1*Δ and *spo77*Δ *ama1*Δ mutants have a complete block in PSM closure (Figure 8B). This stands in contrast to the single mutants, which show reductions, but not a total block in cytokinesis.

How *SPO77*, *SPS1*, and *AMA1* regulate Ssp1 stability is unclear. Because Ama1 is an activator of the APC/C (Cooper *et al.* 2000), it is tempting to speculate that Ama1 is important for the ubiquitination and subsequent degradation of Ssp1, although attempts to see a ubiquitinated form of Ssp1 have not been successful (Maier *et al.* 2007; Diamond *et al.* 2009). We also do not know whether the stabilization of Ssp1 we see in the *sps1*Δ and *spo77*Δ strains reflects a stabilization of the functional pool of Ssp1 at the leading edge. Furthermore, because protein stability is examined at later time points in mutants where the progression through sporulation has been blocked, more studies are needed to determine whether the stabilization of Ssp1 we see is due to a direct effect of the mutated gene or an indirect effect due to other earlier defects.

Although ubiquitinated Ssp1 has not been detected, Ssp1 appears to be phosphorylated (Maier *et al.* 2007). We find that phosphorylation of Ssp1 is reduced in the *sps1*Δ and *spo77*Δ mutants (Figure 8H), although not abolished. Because we see Sps1 and Ssp1 in a complex (Figure 8G), it is possible that Ssp1 is a substrate of Sps1, although studies will need to be done to demonstrate the direct phosphorylation of Ssp1 by Sps1. Since Sps1 is a STE20-like kinase in the GCKIII subfamily (Slubowski *et al.* 2014), it is possible that

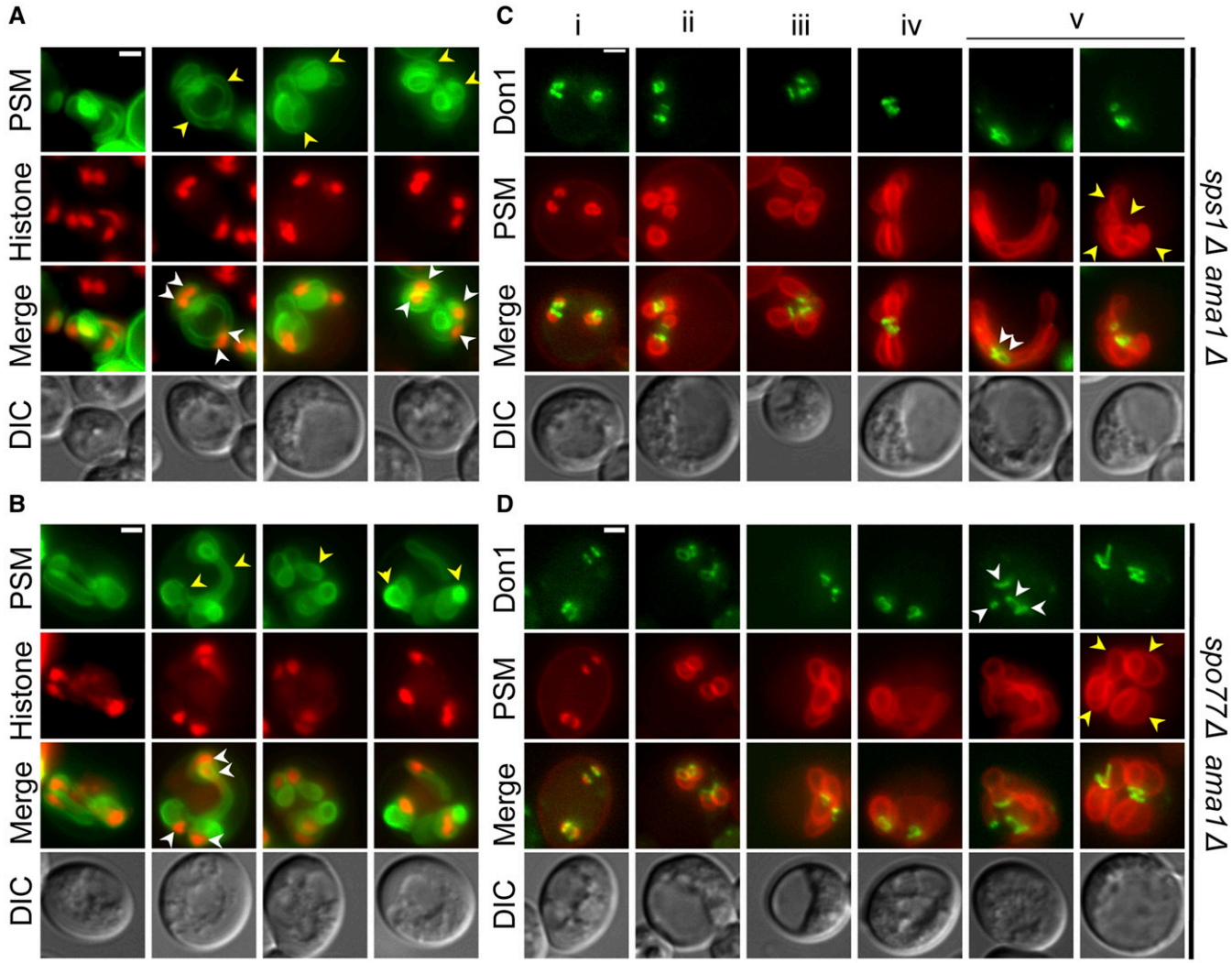

Figure 7 PSM development and Don1 localization in *sps1*Δ *ama1*Δ and *spo77*Δ *ama1*Δ double mutant cells. (A and B) PSM development in *sps1*Δ *ama1*Δ (LH1048) and *spo77*Δ *ama1*Δ (LH1051), with PSMs labeled with GFP-Spo20$^{51–91}$ (Nakanishi *et al.* 2004) and nuclei with Htb2-mCherry. Yellow arrows indicate areas where heavily invaginated PSM material is seen late during spore morphogenesis. White arrows indicate nuclei. (C and D) Don1-GFP localization in *sps1*Δ *ama1*Δ (LH1057) and *spo77*Δ *ama1*Δ (LH1058) strains; PSMs are visualized with a red fluorescent PSM marker, pRS426-R20. In A and B, yellow arrows indicate grossly misshapen PSM structures; white arrows indicate nuclei still contained within PSM material. In C and D, yellow arrows indicate grossly misshapen PSM structures; white arrows indicate intact Don1 rings well after spore appearance in *WT* cells. Bar, 2 μm.

Sps1 phosphorylates Ssp1 along with another kinase that acts in parallel. The functional impact of Ssp1 phosphorylation remains to be determined.

A role for *SPS1* in influencing a cytokinetic event may extend beyond yeast sporulation. An *SPS1* homolog in the amoeba *Dictyostelium discoideum*, SvkA, has been shown to have a role in the final steps of cytokinesis in mitotic division, as well as playing a role in the formation of fruiting bodies in response to starvation (Rohlfs *et al.* 2007). The localization of SvkA is also similar to Sps1 in that both have cytonuclear localization and enrichment at the membrane when cytokinesis occurs (Rohlfs *et al.* 2007), suggesting that Sps1 and related GCKIII kinases may have primordial origins in stress response and influencing cytokinesis in these contexts. Similarly, the *Drosophila* GCKIII kinase Wheezy has been shown to be involved in trachea development, where *wheezy* mutants have inappropriate trafficking of membrane-bound adhesion proteins and increase accumulation of Crumbs protein on the tracheal membrane (Song *et al.* 2013), although Crumbs and Ssp1 do not show any obvious homology.

The timing of prospore membrane closure, as with any cytokinetic event, needs to be properly regulated. The APC/C is a highly regulated complex with direct roles regulating the events that occur during the meiotic division and subject to complex feedback loops (Cooper *et al.* 2000; Oelschlaegel *et al.* 2005; Penkner *et al.* 2005; Tan *et al.* 2010; Tsuchiya *et al.* 2011; Okaz *et al.* 2012). The involvement of *AMA1* in regulating the cytokinetic event suggests a mechanism for regulating the meiotic cell cycle, with APC/C^{AMA1} activity coordinated with other cell cycle events. The involvement of the APC/C in cytokinesis is likely more universal, as

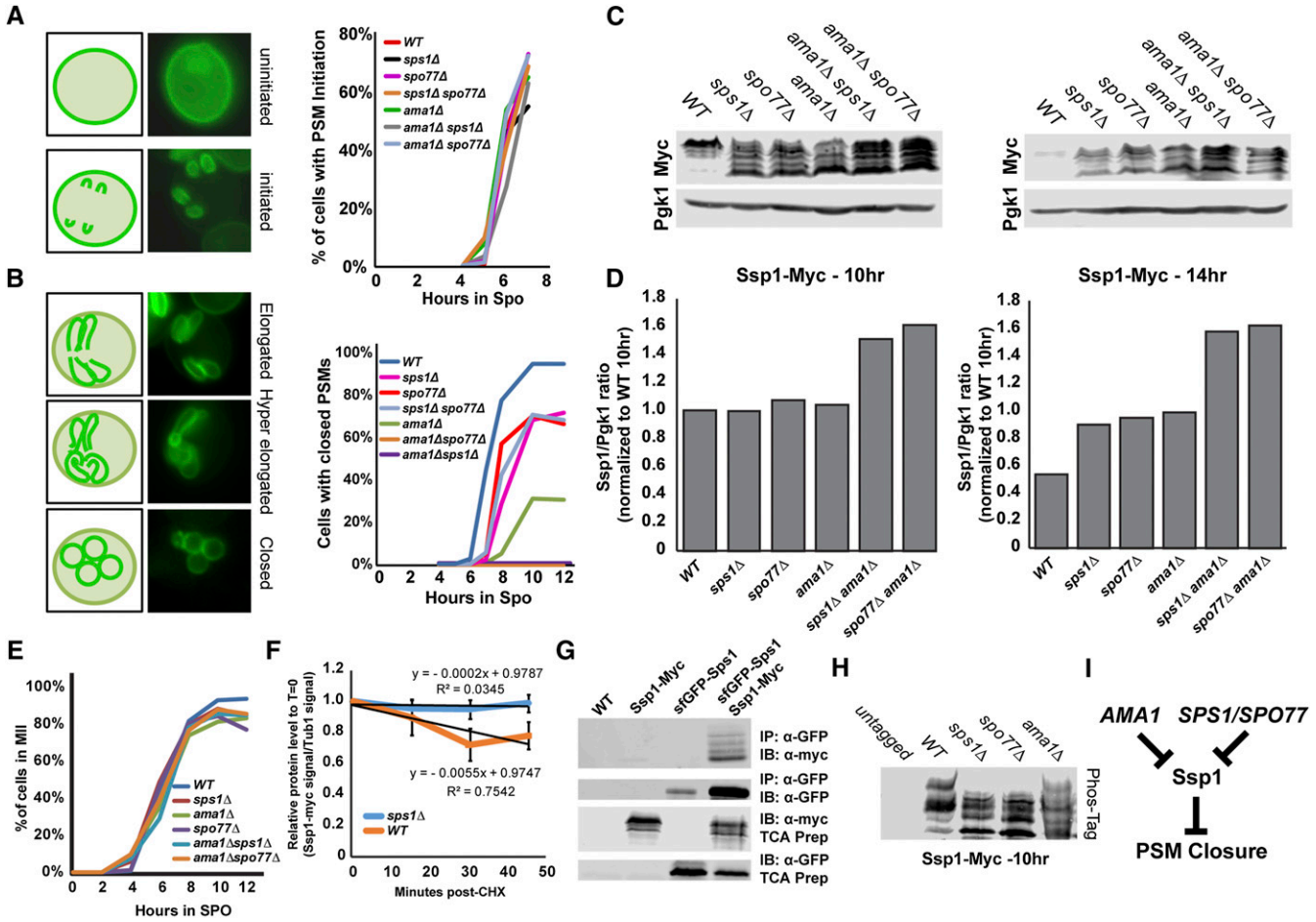

Figure 8 *SPS1* and *SPO77* act together in parallel to *AMA1* to affect Ssp1 stability and phosphorylation. Quantitation of PSM initiation (A) and PSM closure (B) in WT (LH917), *sps1*Δ (LH1047), *spo77*Δ (LH1049), *ama1*Δ (LH1052), *sps1*Δ *spo77*Δ (LH1050), *sps1*Δ *ama1*Δ (LH1048), and *spo77*Δ *ama1*Δ (LH1051) cells. In A, cells were scored for PSM initation and any cell that had forming PSMs were counted as intitiated. In B, cells that had PSMs were counted as either closed (if their PSMs were rounded) or open. Cells were considered to have closed PSMs if the PSMs were rounded. Cells were counted as having open PSMs if PSMs were present and not rounded; hyperelongated PSMs were counted as open. (C) *SPS1* and *SPO77* are required for proper Ssp1 steady state levels. Ssp1-13*x*-myc levels were assayed by immunblotting, from lysates made from samples taken during sporulation, using Ssp1-myc in WT (LH1027), *sps1*Δ (LH1028), *spo77*Δ (LH1030), *ama1*Δ (LH1029), *sps1*Δ *ama1*Δ (LH1031), and *spo77*Δ *ama1*Δ (LH1032) cells. Pgk1 was assayed as a loading control. (D) Blots from C were quantified by normalizing Ssp1-13x-myc signal to the Pgk1 signal (see *Materials and Methods* for details). (E) Kinetics of meiosis, as assayed using Htb2-mCherry, for the cultures used in C. (F) Relative protein stability of Ssp1was assayed in WT (LH1027), sps1Δ (LH1028), and from sporulating cells. Cycloheximide (CHX) was added to cells which were in sporulation media at 8 hr, and samples were withdrawn at the indicated elapsed time after CHX addition. Tub1 was used as a loading control to normalize Ssp1-myc abundance. A *P*-value of 0.049 was calculated using the ANCOVA statistic, indicating a significant difference between the rates of Ssp1-myc loss in the WT and sps1Δ backgrounds. (G) Ssp1 is in a complex with Sps1. Immunoprecipitation experiments were carried out using synchronously sporulating cultures of WT (LH902), Ssp1-13x-myc (LH1027), sfGFP-Sps1 (LH986), and Ssp1-13x-myc/sfGFP-Sps1 (LH1034) cells. (H) An aliquote of the lysates from the 10-hr time point from the blots in C were run on a Phos-tag gel to separate the different phosphor-isoforms of Ssp1. (I) Model of the relationship between *SPS1*, *SPO77*, and *AMA1*. See *Discussion* for details.

the APC/C also plays a role in regulating abscission during cytokinesis by degrading the Plk1 kinase in human cells (Lindon and Pines 2004; Bastos and Barr 2010). Similarly, a meiosis-specific activator of the APC/C (*mfr1*) in *Schizosaccharomyces pombe* has been suggested to coordinate the nuclear divisions in sporulation, suggesting a conserved role for meiosis-specific APC/C activators in meiotic cytokinesis, although a direct role in forespore membrane closure (the *S. pombe* prospore membrane equivalent) for *mfr1* has not been demonstrated (Blanco *et al.* 2001). The activator of Sps1 is not known, and thus the signal to which it is responding is currently unclear. The timing of Sps1 protein accumulation is governed by an Ime2/Rim4-dependent translational repression and derepression that delays Sps1 production until after MII, despite *SPS1* transcription occurring at MI with Ndt80-MSE induction (Berchowitz *et al.* 2013). Whatever activates Sps1 may represent an additional signal monitoring the state of the cell, whose output is used to decide when cytokinesis occurs.

Acknowledgments

We thank Aaron Neiman for the blue fluorescent PSM marker Spo20$^{51-91}$-mTagBFP; Alan Fossa for technical assistance; and Alexey Veraksa, Dang Truong, Catherine McCusker, and Paul Garrity for helpful comments on the manuscript. This work was supported by a Goranson award and a doctoral dissertation grant from the University of Massachusetts, Boston (UMass Boston) to S.M.P. and the following awards to L.S.H.: MCB-0544160 from the National Science Foundation, GM086805 from the National Institutes of Health, and a Proposal Development Grant and a Healy award from UMass Boston.

Literature Cited

Balasubramanian, M. K., E. Bi, and M. Glotzer, 2004 Comparative analysis of cytokinesis in budding yeast, fission yeast and animal cells. Curr. Biol. 14: R806–R818.

Bastos, R. N., and F. A. Barr, 2010 Plk1 negatively regulates Cep55 recruitment to the midbody to ensure orderly abscission. J. Cell Biol. 191: 751–760.

Berchowitz, L. E., A. S. Gajadhar, F. J. van Werven, A. A. De Rosa, M. L. Samoylova *et al.*, 2013 A developmentally regulated translational control pathway establishes the meiotic chromosome segregation pattern. Genes Dev. 27: 2147–2163.

Bi, E., P. Maddox, D. J. Lew, E. D. Salmon, J. N. McMillan *et al.*, 1998 Involvement of an actomyosin contractile ring in *Saccharomyces cerevisiae* cytokinesis. J. Cell Biol. 142: 1301–1312.

Blanco, M. A., L. Pelloquin, and S. Moreno, 2001 Fission yeast mfr1 activates APC and coordinates meiotic nuclear division with sporulation. J. Cell Sci. 114: 2135–2143.

de Boer, M., P. S. Nielsen, J. P. Bebelman, H. Heerikhuizen, H. A. Andersen *et al.*, 2000 Stp1p, Stp2p and Abf1p are involved in regulation of expression of the amino acid transporter gene BAP3 of Saccharomyces cerevisiae. Nucleic Acids Res. 28: 974–981.

Carballido-López, R., 2006 The bacterial actin-like cytoskeleton. Microbiol. Mol. Biol. Rev. 70: 888–909.

Coluccio, A., E. Bogengruber, M. N. Conrad, M. E. Dresser, P. Briza *et al.*, 2004 Morphogenetic pathway of spore wall assembly in Saccharomyces cerevisiae. Eukaryot. Cell 3: 1464–1475.

Cooper, K. F., and R. Strich, 2011 Meiotic control of the APC/C: similarities & differences from mitosis. Cell Div. 6: 16.

Cooper, K. F., M. J. Mallory, D. B. Egeland, M. Jarnik, and R. Strich, 2000 Ama1p is a meiosis-specific regulator of the anaphase promoting complex/cyclosome in yeast. Proc. Natl. Acad. Sci. USA 97: 14548–14553.

Diamond, A. E., J.-S. Park, I. Inoue, H. Tachikawa, and A. M. Neiman, 2009 The anaphase promoting complex targeting subunit Ama1 links meiotic exit to cytokinesis during sporulation in Saccharomyces cerevisiae. Mol. Biol. Cell 20: 134–145.

Friesen, H., R. Lunz, S. Doyle, and J. Segall, 1994 Mutation of the SPS1-encoded protein kinase of Saccharomyces cerevisiae leads to defects in transcription and morphology during spore formation. Genes Dev. 8: 2162–2175.

Gietz, R. D., and R. H. Schiestl, 2007 Large-scale high-efficiency yeast transformation using the LiAc/SS carrier DNA/PEG method. Nat. Protoc. 2: 38–41.

Green, R. A., E. Paluch, and K. Oegema, 2012 Cytokinesis in animal cells. Annu. Rev. Cell Dev. Biol. 28: 29–58.

Holmes, D. S., and M. Quigley, 1981 A rapid boiling method for the preparation of bacterial plasmids. Anal. Biochem. 114: 193–197.

Huang, L. S., H. K. Doherty, and I. Herskowitz, 2005 The Smk1p MAP kinase negatively regulates Gsc2p, a 1,3-beta-glucan synthase, during spore wall morphogenesis in Saccharomyces cerevisiae. Proc. Natl. Acad. Sci. USA 102: 12431–12436.

Iwamoto, M. A., S. R. Fairclough, S. A. Rudge, and J. Engebrecht, 2005 Saccharomyces cerevisiae Sps1p regulates trafficking of enzymes required for spore wall synthesis. Eukaryot. Cell 4: 536–544.

Jones, G. M., J. Stalker, S. Humphray, A. West, T. Cox *et al.*, 2008 A systematic library for comprehensive overexpression screens in Saccharomyces cerevisiae. Nat. Methods 5: 239–241.

Jürgens, G., 2005 Cytokinesis in higher plants. Annu. Rev. Plant Biol. 56: 281–299.

Kane, S. M., and R. Roth, 1974 Carbohydrate metabolism during ascospore development in yeast. J. Bacteriol. 118: 8–14.

Kinoshita, E., E. Kinoshita-Kikuta, K. Takiyama, and T. Koike, 2006 Phosphate-binding tag, a new tool to visualize phosphorylated proteins. Mol. Cell. Proteomics 5: 749–757.

Knop, M., and K. Strasser, 2000 Role of the spindle pole body of yeast in mediating assembly of the prospore membrane during meiosis. EMBO J. 19: 3657–3667.

Krishnamoorthy, T., X. Chen, J. Govin, W. L. Cheung, J. Dorsey *et al.*, 2006 Phosphorylation of histone H4 Ser1 regulates sporulation in yeast and is conserved in fly and mouse spermatogenesis. Genes Dev. 20: 2580–2592.

Lam, C., E. Santore, E. Lavoie, L. Needleman, N. Fiacco *et al.*, 2014 A visual screen of protein localization during sporulation identifies new components of prospore membrane-associated complexes in budding yeast. Eukaryot. Cell 13: 383–391.

Lee, D. M., and T. J. C. Harris, 2014 Coordinating the cytoskeleton and endocytosis for regulated plasma membrane growth in the early Drosophila embryo. BioArchitecture 4: 68–74.

Lee, S., W. A. Lim, and K. S. Thorn, 2013 Improved blue, green, and red fluorescent protein tagging vectors for S. cerevisiae. PLoS One 8: e67902.

Lin, C. P.-C., C. Kim, S. O. Smith, and A. M. Neiman, 2013 A highly redundant gene network controls assembly of the outer spore wall in S. cerevisiae. PLoS Genet. 9: e1003700.

Lindon, C., and J. Pines, 2004 Ordered proteolysis in anaphase inactivates Plk1 to contribute to proper mitotic exit in human cells. J. Cell Biol. 164: 233–241.

Longtine, M. S., A. McKenzie, D. J. Demarini, N. G. Shah, A. Wach *et al.*, 1998 Additional modules for versatile and economical PCR-based gene deletion and modification in Saccharomyces cerevisiae. Yeast 14: 953–961.

Maier, P., N. Rathfelder, M. G. Finkbeiner, C. Taxis, M. Mazza *et al.*, 2007 Cytokinesis in yeast meiosis depends on the regulated removal of Ssp1p from the prospore membrane. EMBO J. 26: 1843–1852.

McLean, J. R., D. Chaix, M. D. Ohi, and K. L. Gould, 2011 State of the APC/C: organization, function, and structure. Crit. Rev. Biochem. Mol. Biol. 46: 118–136.

Moens, P. B., 1971 Fine structure of ascospore development in the yeast Saccharomyces cerevisiae. Can. J. Microbiol. 17: 507–510.

Moreno-Borchart, A. C., K. Strasser, M. G. Finkbeiner, A. Shevchenko, and M. Knop, 2001 Prospore membrane formation linked to the leading edge protein (LEP) coat assembly. EMBO J. 20: 6946–6957.

Nag, D. K., M. P. Koonce, and J. Axelrod, 1997 SSP1, a gene necessary for proper completion of meiotic divisions and spore formation in Saccharomyces cerevisiae. Mol. Cell. Biol. 17: 7029–7039.

Nakanishi, H., P. de los Santos, and A. M. Neiman, 2004 Positive and negative regulation of a SNARE protein by control of intracellular localization. Mol. Biol. Cell 15: 1802–1815.

Neiman, A. M., 1998 Prospore membrane formation defines a developmentally regulated branch of the secretory pathway in yeast. J. Cell Biol. 140: 29–37.
Neiman, A. M., 2011 Sporulation in the budding yeast Saccharomyces cerevisiae. Genetics 189: 737–765.
Nickas, M. E., and A. M. Neiman, 2002 Ady3p links spindle pole body function to spore wall synthesis in Saccharomyces cerevisiae. Genetics 160: 1439–1450.
Oelschlaegel, T., M. Schwickart, J. Matos, A. Bogdanova, A. Camasses *et al.*, 2005 The yeast APC/C subunit Mnd2 prevents premature sister chromatid separation triggered by the meiosis-specific APC/C-Ama1. Cell 120: 773–788.
Okaz, E., O. Argüello-Miranda, A. Bogdanova, P. K. Vinod, J. J. Lipp *et al.*, 2012 Meiotic prophase requires proteolysis of M phase regulators mediated by the meiosis-specific APC/C Ama1. Cell 151: 603–618.
Park, J.-S., Y. Okumura, H. Tachikawa, and A. M. Neiman, 2013 SPO71 encodes a developmental stage-specific partner for Vps13 in Saccharomyces cerevisiae. Eukaryot. Cell 12: 1530–1537.
Parodi, E. M., C. S. Baker, C. Tetzlaff, S. Villahermosa, and L. S. Huang, 2012 SPO71 mediates prospore membrane size and maturation in Saccharomyces cerevisiae. Eukaryot. Cell 11: 1191–1200.
Penkner, A. M., S. Prinz, S. Ferscha, and F. Klein, 2005 Mnd2, an essential antagonist of the anaphase-promoting complex during meiotic prophase. Cell 120: 789–801.
Percival-Smith, A., and J. Segall, 1986 Characterization and mutational analysis of a cluster of three genes expressed preferentially during sporulation of Saccharomyces cerevisiae. Mol. Cell. Biol. 6: 2443–2451.
Pesin, J. A., and T. L. Orr-Weaver, 2008 Regulation of APC/C activators in mitosis and meiosis. Annu. Rev. Cell Dev. Biol. 24: 475–499.
Philips, J., and I. Herskowitz, 1998 Identification of Kel1p, a Kelch domain-containing protein involved in cell fusion and morphology in Saccharomyces cerevisiae. J. Cell Biol. 143: 375–398.
Pollard, T. D., and J.-Q. Wu, 2010 Understanding cytokinesis: lessons from fission yeast. Nat. Rev. Mol. Cell Biol. 11: 149–155.
Rabitsch, K. P., A. Tóth, M. Gálová, A. Schleiffer, G. Schaffner *et al.*, 2001 A screen for genes required for meiosis and spore formation based on whole-genome expression. Curr. Biol. 11: 1001–1009.
Rohlfs, M., R. Arasada, P. Batsios, J. Janzen, and M. Schleicher, 2007 The Ste20-like kinase SvkA of Dictyostelium discoideum is essential for late stages of cytokinesis. J. Cell Sci. 120: 4345–4354.
Rolli, E., E. Ragni, M. de Medina-Redondo, J. Arroyo, C. R. V. de Aldana *et al.*, 2011 Expression, stability, and replacement of glucan-remodeling enzymes during developmental transitions in Saccharomyces cerevisiae. Mol. Biol. Cell 22: 1585–1598.
Rose, M. D., and G. R. Fink, 1990 Methods in Yeast Genetics, Cold Spring Harbor, NY: Cold Spring Harbor Laboratory Press.
Schneider, C. A., W. S. Rasband, and K. W. Eliceiri, 2005 NIH Image to ImageJ: 25 years of image analysis. Nat. Methods 2: 905–909.
Sikorski, R. S., and P. Hieter, 1989 A system of shuttle vectors and yeast host strains designed for efficient manipulation of DNA in Saccharomyces cerevisiae. Genetics 122: 19–27.
Slubowski, C. J., S. M. Paulissen, and L. S. Huang, 2014 The GCKIII kinase Sps1 and the 14–3-3 Isoforms, Bmh1 and Bmh2, cooperate to ensure proper sporulation in Saccharomyces cerevisiae. PLoS One 9: e113528.
Slubowski, C. J., A. D. Funk, J. M. Roesner, S. M. Paulissen, and L. S. Huang, 2015 Plasmids for C-terminal tagging in Saccharomyces cerevisiae that contain improved GFP proteins, Envy and Ivy. Yeast 32: 379–387.
Song, Y., M. Eng, and A. S. Ghabrial, 2013 Focal defects in single-celled tubes mutant for Cerebral cavernous malformation3, GCKIII, or NSF2. Dev. Cell 25: 507–519.
Tan, G. S., J. Magurno, and K. F. Cooper, 2010 Ama1p-activated anaphase-promoting complex regulates the destruction of Cdc20p during meiosis II. Mol. Biol. Cell 22: 315–326.
Taxis, C., C. Maeder, S. Reber, N. Rathfelder, K. Miura *et al.*, 2006 Dynamic organization of the actin cytoskeleton during meiosis and spore formation in budding yeast. Traffic 7: 1628–1642.
Tsuchiya, D., C. Gonzalez, and S. Lacefield, 2011 The spindle checkpoint protein Mad2 regulates APC/C activity during prometaphase and metaphase of meiosis I in Saccharomyces cerevisiae. Mol. Biol. Cell 22: 2848–2861.
Wheeler, R. J., N. Scheumann, B. Wickstead, K. Gull, and S. Vaughan, 2013 Cytokinesis in Trypanosoma brucei differs between bloodstream and tsetse trypomastigote forms: implications for microtubule-based morphogenesis and mutant analysis. Mol. Microbiol. 90: 1339–1355.
Whinston, E., G. Omerza, A. Singh, C. W. Tio, and E. Winter, 2013 Activation of the Smk1 mitogen-activated protein kinase by developmentally regulated autophosphorylation. Mol. Cell. Biol. 33: 688–700.

Communicating editor: O. Cohen-Fix

GENETICS

Supporting Information
www.genetics.org/lookup/suppl/doi:10.1534/genetics.115.183939/-/DC1

Timely Closure of the Prospore Membrane Requires *SPS1* and *SPO77* in *Saccharomyces cerevisiae*

Scott M. Paulissen, Christian J. Slubowski, Joseph M. Roesner, and Linda S. Huang

DOI: 10.1534/genetics.115.183939

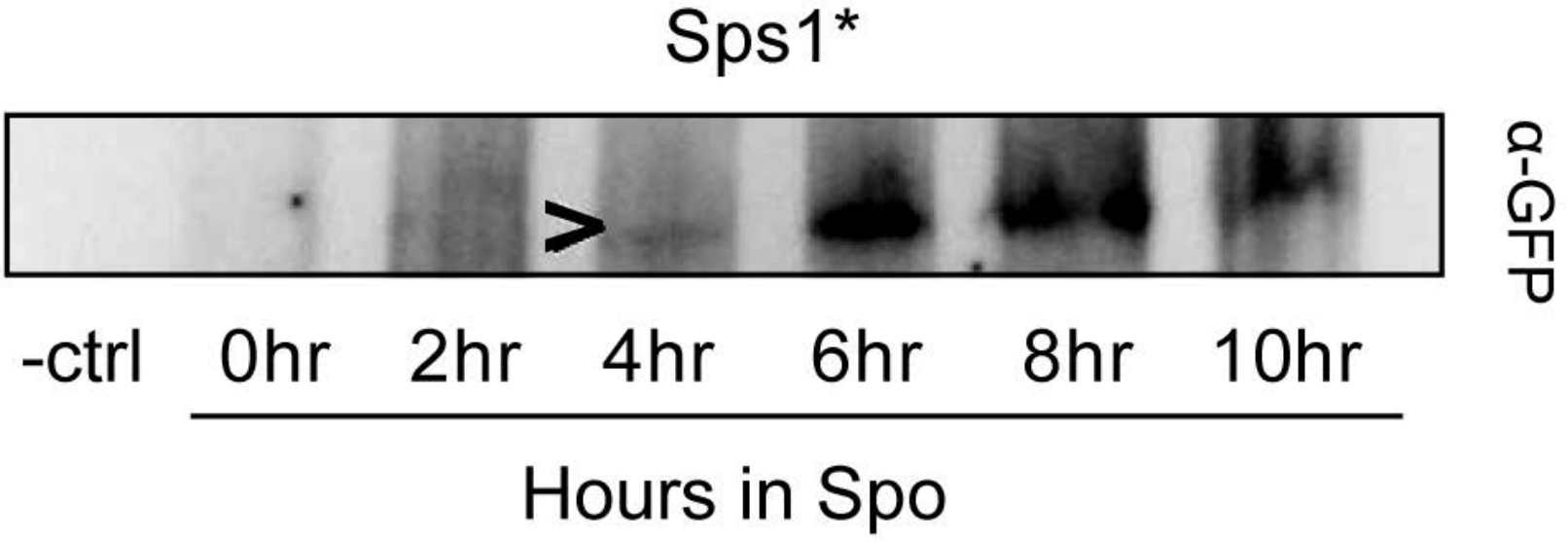

Figure S1. The Sps1-3xGFP fusion protein is expressed. Cells expressing the *sps1** were sporulated and lysates were prepared from the samples for Western blot analysis. Time indicates the time cells have been in sporulation media. -ctrl sample shows lysates from an untagged *SPS1* strain.

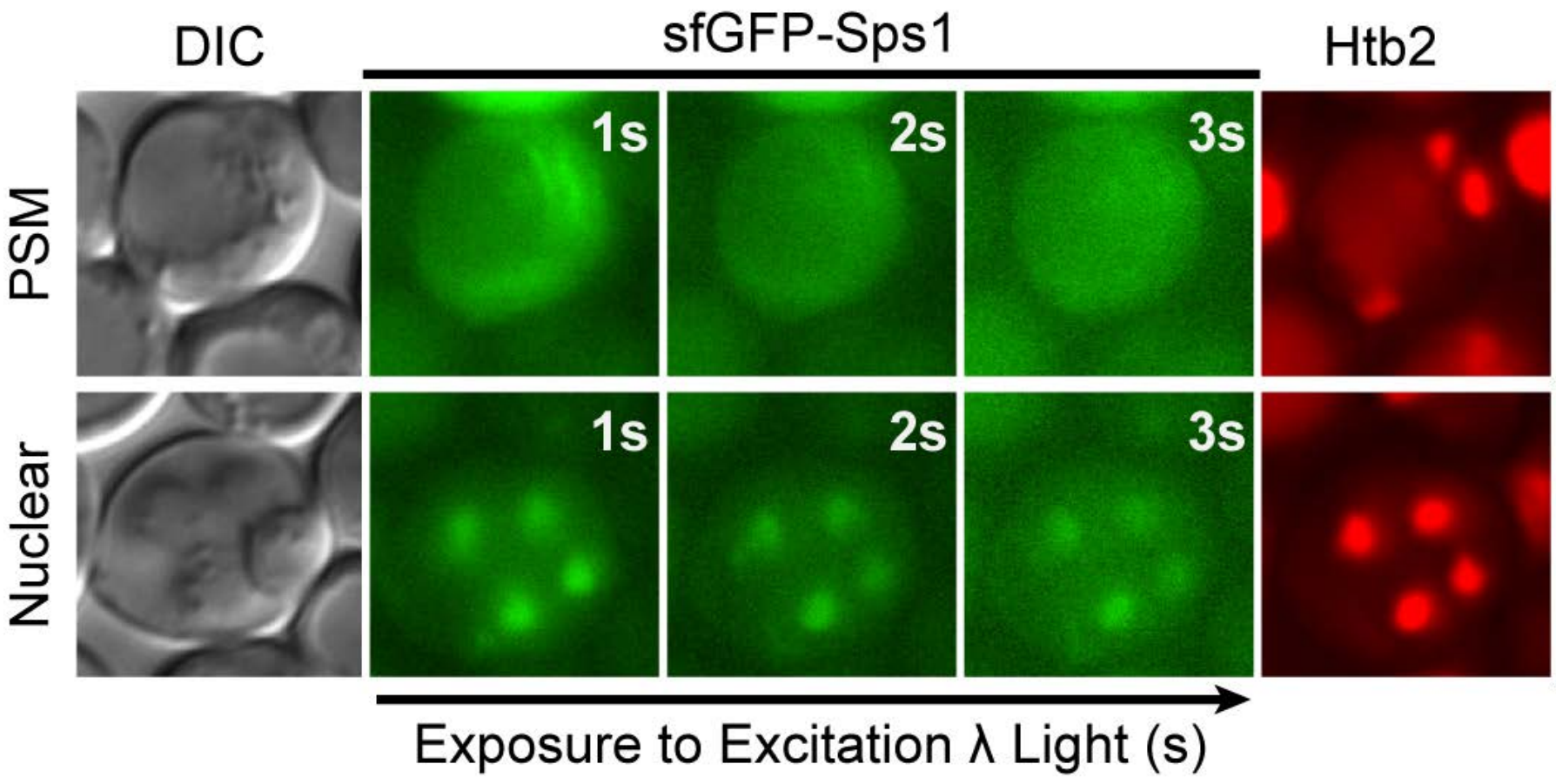

Figure S2. sfGFP-Sps1 photobleaches rapidly under illumination. Two live sporulating cells (LH986) imaged over three sequential exposures times immediately after illumination. Top row shows a cell with sfGFP-Sps1 with PSM localization. Bottom row shows a cell with sfGFP-Sps1 localizing to the nucleus. Nuclei are visualized using Htb2-mCherry. Exposure time was 1.000s for each image. Note the loss of PSM fluorescence after only 1s of illumination while nuclear fluorescence can still be seen.

TABLE S1: Yeast Strains

Strain	Genotype	Source
LH177	MAT**a**/MATα *ho::LYS2/ho::LYS2 lys2/lys2 ura3/ura3 leu2/leu2 his3/his3 trp1ΔFA/trp1ΔFA*	Huang *et al.* 2005
LH790	MAT**a**/MATα *ho::LYS2/ho::LYS2 lys2/lys2 ura3/ura3 leu2/leu2 his3/his3 trp1ΔFA/trp1ΔFA DON1-GFP-HIS3MX6/DON1-GFP-HIS3MX6*	Parodi *et al.* 2012
LH872	MAT**a**/MATα *ho::LYS2/ho::LYS2 lys2/lys2 ura3/ura3 leu2/leu2 his3/his3 trp1ΔFA/trp1ΔFA sps1::LEU2$^{C.g.}$/sps1::LEU2$^{C.g.}$*	Slubowski *et al*. 2014
LH902	MAT**a**/MATα *ho::LYS2/ho::LYS2 lys2/lys2 ura3/ura3 leu2/leu2 his3/his3 trp1ΔFA/trp1ΔFA HTB2:mCherry:TRP1$^{C.g.}$/HTB2:mCherry:TRP1$^{C.g.}$*	Parodi *et al.* 2012
LH976	MAT**a**/MATα *ho::LYS2/ho::LYS2 lys2/lys2 ura3/ura3 leu2/leu2 his3/his3 trp1ΔFA/trp1ΔFA sps1::HIS3/sps1::HIS3 HTB2:mCherry:TRP1$^{C.g.}$/HTB2:mCherry:TRP1$^{C.g.}$*	Slubowski *et al.* 2014
LH986	MAT**a**/MATα *ho::LYS2/ho::LYS2 lys2/lys2 ura3/ura3 leu2/leu2 his3/his3 trp1ΔFA/trp1ΔFA sfGFP:SPS1/sfGFP:SPS1 HTB2:mCherry:TRP1$^{C.g.}$/HTB2:mCherry:TRP1$^{C.g.}$*	Slubowski *et al*. 2014
LH1010	MAT**a**/MATα *ho::LYS2/ho::LYS2 lys2/lys2 ura3/ura3 leu2/leu2 his3/his3 trp1ΔFA/trp1ΔFA spo77::HIS3$^{C.g.}$/ spo77::HIS3$^{C.g.}$ HTB2:mCherry:TRP1$^{C.g.}$/HTB2:mCherry:TRP1$^{C.g.}$*	This study
LH1011	MAT**a**/MATα *ho::LYS2/ho::LYS2 lys2/lys2 ura3/ura3 leu2/leu2 his3/his3 trp1ΔFA/trp1ΔFA HTB2:mCherry:TRP1$^{C.g.}$/HTB2:mCherry:TRP1$^{C.g.}$ sps1::LEU2/sps1::LEU2 ama1::TRP1$^{C.g.}$/ama1::TRP1$^{C.g.}$*	This study
LH1012	MAT**a**/MATα *ho::LYS2/ho::LYS2 lys2/lys2 ura3/ura3 leu2/leu2 his3/his3 trp1ΔFA/trp1ΔFA sps1:::HIS3MX6/sps1:::HIS3MX6 spo77::HIS3$^{C.g.}$/spo77::HIS3$^{C.g.}$ HTB2:mCherry:TRP1$^{C.g.}$/HTB2:mCherry:TRP1$^{C.g.}$*	This study
LH1013	MAT**a**/MATα *ho::LYS2/ho::LYS2 lys2/lys2 ura3/ura3 leu2/leu2 his3/his3 trp1ΔFA/trp1ΔFA ama1::TRP1$^{C.g.}$/ama1::TRP1$^{C.g.}$ spo77::HIS3$^{C.g.}$/spo77::HIS3$^{C.g.}$ HTB2:mCherry:TRP1$^{C.g.}$/HTB2:mCherry:TRP1$^{C.g.}$*	This study
LH1014	MAT**a**/MATα *ho::LYS2/ho::LYS2 lys2/lys2 ura3/ura3 leu2/leu2 his3/his3 trp1ΔFA/trp1ΔFA ama1::TRP1$^{C.g.}$/ama1::TRP1$^{C.g.}$ HTB2:mCherry:TRP1$^{C.g.}$/HTB2:mCherry:TRP1$^{C.g.}$*	This study
LH1015	MAT**a**/MATα *ho::LYS2/ho::LYS2 lys2/lys2 ura3/ura3 leu2/leu2 his3/his3 trp1ΔFA/trp1ΔFA sps1::LEU2/sps1::LEU2*	
LH1016	MAT**a**/MATα *ho::LYS2/ho::LYS2 lys2/lys2 ura3/ura3 leu2/leu2 his3/his3 trp1ΔFA/trp1ΔFA stp2::HIS3$^{C.g.}$/stp2::HIS3$^{C.g.}$ HTB2:mCherry:TRP1$^{C.g.}$/HTB2:mCherry:TRP1$^{C.g.}$*	This study
LH1017	MAT**a**/MATα *ho::LYS2/ho::LYS2 lys2/lys2 ura3/ura3 leu2/leu2 his3/his3 trp1ΔFA/trp1ΔFA sps1::LEU2$^{C.g.}$/SPS1*	This study
LH1018	MAT**a**/MATα *ho::LYS2/ho::LYS2 lys2/lys2 ura3/ura3 leu2/leu2 his3/his3 trp1ΔFA/trp1ΔFA sps1::LEU2$^{C.g.}$/ sps1:3xGFP:KANMX6*	This study
LH1019	MAT**a**/MATα *ho::LYS2/ho::LYS2 lys2/lys2 ura3/ura3 leu2/leu2 his3/his3 trp1ΔFA/trp1ΔFA sps1:3xGFP:KANMX6/sps1:3xGFP:KANMX6*	This study
LH1020	MAT**a**/MATα *ho::LYS2/ho::LYS2 lys2/lys2 ura3/ura3 leu2/leu2 his3/his3 trp1ΔFA/trp1ΔFA sps1:3xGFP:KANMX6/SPS1*	This study
LH1021	MAT**a**/MATα *ho::LYS2/ho::LYS2 lys2/lys2 ura3/ura3 leu2/leu2 his3/his3 trp1ΔFA/trp1ΔFA sps1:3xGFP:KANMX6/sps1:3xGFP:KANMX6 HTB2:mCherry:TRP1$^{C.g.}$/HTB2:mCherry:TRP1$^{C.g.}$*	This study
LH1022	MAT**a**/MATα *ho::LYS2/ho::LYS2 lys2/lys2 ura3/ura3 leu2/leu2 his3/his3 trp1ΔFA/trp1ΔFA sps1::LEU2/sps1::LEU2 DON1-GFP-HIS3MX6/DON1-GFP-HIS3MX6*	This study
LH1023	MAT**a**/MATα *ho::LYS2/ho::LYS2 lys2/lys2 ura3/ura3 leu2/leu2 his3/his3 trp1ΔFA/trp1ΔFA spo77::HIS3$^{C.g.}$/spo77::HIS3$^{C.g.}$ DON1-GFP-HIS3MX6/DON1-GFP-HIS3MX6*	This study

TABLE S1, continued

Strain	Genotype	Source
LH1024	MAT**a**/MATα *ho::LYS2/ho::LYS2 lys2/lys2 ura3/ura3 leu2/leu2 his3/his3 trp1ΔFA/trp1ΔFA ama1::TRP1$^{C.g.}$/ama1::TRP1$^{C.g.}$ DON1-GFP-HIS3MX6/DON1-GFP-HIS3MX6*	This study
LH1025	MAT**a**/MATα *ho::LYS2/ho::LYS2 lys2/lys2 ura3/ura3 leu2/leu2 his3/his3 trp1ΔFA/trp1ΔFA sps1::LEU2/sps1::LEU2 ama1::TRP1$^{C.g.}$/ama1::TRP1$^{C.g.}$ DON1-GFP-HIS3MX6/DON1-GFP-HIS3MX6*	This study
LH1026	MAT**a**/MATα *ho::LYS2/ho::LYS2 lys2/lys2 ura3/ura3 leu2/leu2 his3/his3 trp1ΔFA/trp1ΔFA spo77::HIS3$^{C.g.}$/spo77::HIS3$^{C.g.}$ ama1::TRP1$^{C.g.}$/ama1::TRP1$^{C.g.}$ DON1-GFP-HIS3MX6/DON1-GFP-HIS3MX6*	This study
LH1027	MAT**a**/MATα *ho::LYS2/ho::LYS2 lys2/lys2 ura3/ura3 leu2/leu2 his3/his3 trp1ΔFA/trp1ΔFA SSP1:13xMYC:TRP1/SSP1:13xMYC:TRP1 HTB2:mCherry:TRP1$^{C.g.}$/HTB2:mCherry:TRP1$^{C.g.}$*	This study
LH1028	MAT**a**/MATα *ho::LYS2/ho::LYS2 lys2/lys2 ura3/ura3 leu2/leu2 his3/his3 trp1ΔFA/trp1ΔFA SSP1:13xMYC:TRP1/SSP1:13xMYC:TRP1 HTB2:mCherry:TRP1$^{C.g.}$/HTB2:mCherry:TRP1$^{C.g.}$ sps1::LEU2$^{C.g.}$/sps1::LEU2$^{C.g.}$*	This study
LH1029	MAT**a**/MATα *ho::LYS2/ho::LYS2 lys2/lys2 ura3/ura3 leu2/leu2 his3/his3 trp1ΔFA/trp1ΔFA SSP1:13xMYC:TRP1/SSP1:13xMYC:TRP1 HTB2:mCherry:TRP1$^{C.g.}$/HTB2:mCherry:TRP1$^{C.g.}$ ama1::TRP1$^{C.g.}$/ama1::TRP1$^{C.g.}$*	This study
LH1030	MAT**a**/MATα *ho::LYS2/ho::LYS2 lys2/lys2 ura3/ura3 leu2/leu2 his3/his3 trp1ΔFA/trp1ΔFA SSP1:13MYC:TRP1/SSP1:13MYC:TRP1 HTB2:mCherry:TRP1$^{C.g.}$/HTB2:mCherry:TRP1$^{C.g.}$ spo77::HIS3$^{C.g.}$/spo77::HIS3$^{C.g.}$*	This study
LH1031	MAT**a**/MATα *ho::LYS2/ho::LYS2 lys2/lys2 ura3/ura3 leu2/leu2 his3/his3 trp1ΔFA/trp1ΔFA SSP1:13xMYC:TRP1/SSP1:13xMYC:TRP1 HTB2:mCherry:TRP1$^{C.g.}$/HTB2:mCherry:TRP1$^{C.g.}$ sps1::LEU2/sps1::LEU2 ama1::TRP1$^{C.g.}$/ama1::TRP1$^{C.g.}$*	This study
LH1032	MAT**a**/MATα *ho::LYS2/ho::LYS2 lys2/lys2 ura3/ura3 leu2/leu2 his3/his3 trp1ΔFA/trp1ΔFA SSP1:13xMYC:TRP1/SSP1:13xMYC:TRP1 HTB2:mCherry:TRP1$^{C.g.}$/HTB2:mCherry:TRP1$^{C.g.}$ spo77::HIS3$^{C.g.}$/spo77::HIS3$^{C.g.}$ ama1::TRP1$^{C.g.}$/ama1::TRP1$^{C.g.}$*	This study
LH1033	MAT**a**/MATα *ho::LYS2/ho::LYS2 lys2/lys2 ura3/ura3 leu2/leu2 his3/his3 trp1ΔFA/trp1ΔFA sfGFP:SPS1/sfGFP:SPS1 spo77::HIS3$^{C.g.}$/spo77::HIS3$^{C.g.}$ HTB2:mCherry:TRP1$^{C.g.}$/HTB2:mCherry:TRP1$^{C.g.}$*	This study
LH1034	MAT**a**/MATα *ho::LYS2/ho::LYS2 lys2/lys2 ura3/ura3 leu2/leu2 his3/his3 trp1ΔFA/trp1ΔFA sfGFP:SPS1/sfGFP:SPS1 SSP1:13xMYC:TRP1/SSP1:13xMYC:TRP1 HTB2:mCherry:TRP1$^{C.g.}$/HTB2:mCherry:TRP1$^{C.g.}$*	This study

TABLE S2: Yeast Strains Containing Plasmids

Strain	Genotype	Source
	Strains for screen	
LH1034	LH1021 plus pGP564-YGPM1j19	This study
LH1035	LH1021 plus pGP564-YGPM4k18	This study
LH1036	LH1021 plus pGP564-YGPM30n09	This study
LH1037	LH1021 plus pGP564-YGPM27a08	This study
LH1038	LH1021 plus pRS423-*SPO77*	This study
LH1039	LH1021 plus pRS423-*STP2*	This study
LH1040	LH1021 plus pRS423	This study
LH1041	LH976 plus pGP564	This study
LH1042	LH976 plus pGP564-YGPM4k18	This study
LH1043	LH976 plus pGP564-YGPM1j19	This study
LH1044	LH1010 plus pGP564	This study
LH1045	LH1010 plus pGP564-YGPM4k18	This study
LH1046	LH1010 plus pGP564-YGPM1j19	This study
LH1060	LH1021 plus pRS426-G20	This study
	Strains for visualizing PSM	
LH917	LH902 plus pRS426-G20	Parodi et al 2012
LH1047	LH976 plus pRS426-G20	This study
LH1048	LH1011 plus pRS426-G20	This study
LH1049	LH1010 plus pRS426-G20	This study
LH1050	LH1012 plus pRS426-G20	This study
LH1051	LH1013 plus pRS426-G20	This study
LH1052	LH1014 plus pRS426-G20	This study
	Strains for visualizing LEP and PSM	
LH1053	LH790 plus pRS426-R20	This study
LH1054	LH1022 plus pRS426-R20	This study
LH1055	LH1024 plus pRS426-R20	This study
LH1056	LH1023 plus pRS426-R20	This study
LH1057	LH1025 plus pRS426-R20	This study
LH1058	LH1026 plus pRS426-R20	This study
	Strain for localizing Sps1	
LH1059	LH872 plus pCS232 (pRS424-prSPS1-Envy-*SPS1*) and pRS426-B20	This study

Table S3: Primer List

Locus/ Plasmid	Template	Primer Name	Sequence (5' to 3')
sps1-3xGFP: kanMX6	pFA6a-3xGFP: kanMX6	OLH728	GAAGAGATCTCACTAAGAATTGAAGCAATAAAGAAAGG ATTCGTTcggatccccgggttaattaa
		OLH784	AACTCAAGCATATACACATATTATATATATATATCTATTT TTTTAgaattcgagctcgtttaaac
spo77:: *HIS3*$^{C.g.}$	pCg*HIS3*	OLH1098	CTTGCAGTATTTCTATGTTCCTTAAGAGATCAATAGAAG TAGAATcacaggaaacagctatgacc
		OLH1099	GCTAATTGTGTAGATGTTTGCATGCCGCGGTTTTATCG CTGCGTCAgttgtaaaacgacggccagt
pRS423-*SPS1*	pGP564-YGPM1j19	OLH1332	GATctcgagGAGCTGTCCCAGGTTCGG
		OLH1333	GATgagctcCGCATCAATGACGGGACAG
pRS423-*SPO77*	pGP564-YGPM4k18	OLH1253	CGGctcgagTGTACTGTCCGGTTCCTTGC
		OLH1254	CGCgagctcTTCGAGAAATGGAGAACTTCG
pRS423-*STP2*	pGP564-YGPM30n09	OLH1241	CGGctcgagGCATTGATTTCCCAATTCGT
		OLH1242	CGCgatcgatATACACCTCTGGATTATTGATGTG
SSP1-13x myc: *TRP1*	pFA6a-13x myc: *TRP1*	OLH1026	GATGCAAAACAAAACTTGGATGAAAACGTCTGGAGAA CTCCTATcggatccccgggttaattaa
		OLH1027	AGCATAGAACATGGAATGAGTGTTCAAACTATATTCG TTTGTTTTgaattcgagctcgtttaaac
stp2::*HIS3*$^{C.g.}$	pCg*HIS3*	OLH1152	AGTGATTAATCATCCGACAAACAGACAAATGCAAGAGAGC cacaggaaacagctatgacc
		OLH1153	TTACGTAAAATACCTGAAACCGCCATAAAAATAATACCTG gttgtaaaacgacggccagt
pCS54	WT genomic DNA	OLH1230	TGCATTCAAATGTAGATTCAGC
		OLH1257	ATTCAGAATTCTTTGTGCTATTTTCTTTTGTTGTTTAG
pCS208	pFA6a-link-Envy-Sp*HIS5*	OLH1493	AGTAGAGCTCGAATTCATGTCTAAAGGCGAGGAATTG
		OLH1494	CAACGGTACCAAGCTTTTTGTACAATTCGTCCATTCCTAA TG

Table S4: Plasmids used in this study

Plasmid Name	Description	Source
pFA6a-3xGFP:kanMX6	3xGFP C-terminal tagging vector	Koval *et al.* 2005
pRS423	pRS423 (*HIS3* marked)	Sikorski and Hieter 1989
pRS423-*SPS1*	*SPS1* overexpression vector	This study
pRS423-*SPO77*	*SPO77* overexpression vector	This study
pRS423-*STP2*	*STP2* overexpression vector	This study
pRS426-G20	GFP-spo20$^{51\text{-}90}$	Nakanishi *et al.* 2006
pRS426-R20	mRFP-spo20$^{51\text{-}90}$	Diamond *et al.* 2009
pRS426-B20	spo20$^{51\text{-}90}$-mTagBFP	Lin *et al.* 2013
pGP564	pGP564 (*LEU2* marked)	Jones *et al.* 2008
pGP564-YGPM1j19	Library plasmid containing *SPS1* and other genes	Jones *et al.* 2008
pGP564-YGPM4k18	Library plasmid containing *SPO77* and other genes	Jones *et al.* 2008
pGP564-YGPM27a08	Library plasmid containing part of *TRA1*	Jones *et al.* 2008
pGP564-YGPM30n09	Library plasmid containing *STP2* and other genes	Jones *et al.* 2008
pCg*His3*	*HIS3*$^{C.g.}$ for gene knock outs	Kenji Irie
pFA6a-13xmyc:TRP1	13xmyc C-terminal tagging vector	Longtine *et al.* 1995
pFA6a-link-Envy-Sp*HIS5*	Envy C-terminal tagging vector	Slubowski *et al.* 2015
pCS99 (pRS316-prTEF2-GFP-SPS1)	pTEF2 GFP-*SPS1* expression vector	Slubowski *et al.* 2014
pCS232 (pRS424-prSPS1-Envy-SPS1)	pSPS1 Envy-*SPS1* expression vector	This Study
pRS424	pRS424 (*TRP1* marked)	Sikorski and Hieter 1989

File S1. A ±45° 3D projection of a representative wild type cell during early PSM growth. (.mov, 714 KB)

Available for download as a .mov file at
www.genetics.org/lookup/suppl/doi:10.1534/genetics.115.183939/-/DC1/FileS1.mov

File S2. A ±45° 3D projection of a representative *sps1Δ* cell during early PSM growth. (.mov, 3,376 KB)

Available for download as a .mov file at
www.genetics.org/lookup/suppl/doi:10.1534/genetics.115.183939/-/DC1/FileS2.mov

File S3. A ±45° 3D projection of a representative *spo77Δ* cell during early PSM growth. (.mov, 1,085 KB)

Available for download as a .mov file at
www.genetics.org/lookup/suppl/doi:10.1534/genetics.115.183939/-/DC1/FileS3.mov

File S4. A ±45° 3D projection of a representative wild type cell during late PSM development. (.mov, 1,335 KB)

Available for download as a .mov file at
www.genetics.org/lookup/suppl/doi:10.1534/genetics.115.183939/-/DC1/FileS4.mov

File S5. A ±45° 3D projection of a representative *sps1Δ* cell during late PSM development. (.mov, 1,476 KB)

Available for download as a .mov file at
www.genetics.org/lookup/suppl/doi:10.1534/genetics.115.183939/-/DC1/FileS5.mov

File S6. A ±45° 3D projection of a representative *spo77Δ* cell during late PSM development. (.mov, 2,256 KB)

Available for download as a .mov file at
www.genetics.org/lookup/suppl/doi:10.1534/genetics.115.183939/-/DC1/FileS6.mov

File S7. A time lapse video of a representative wild type cell (LH917) showing the normal closure kinetics of the PSM. (.mov, 370 KB)

Available for download as a .mov file at
www.genetics.org/lookup/suppl/doi:10.1534/genetics.115.183939/-/DC1/FileS7.mov

File S8. A time lapse video of a representative *sps1Δ* cell (LH1047) showing the closure kinetics of the PSM. (.mov, 1,004 KB)

Available for download as a .mov file at
www.genetics.org/lookup/suppl/doi:10.1534/genetics.115.183939/-/DC1/FileS8.mov

File S9. A time lapse video of a representative *spo77Δ* cell (LH1049) showing the closure kinetics of the PSM. (.mov, 1,208 KB)

Available for download as a .mov file at
www.genetics.org/lookup/suppl/doi:10.1534/genetics.115.183939/-/DC1/FileS9.mov

Supplemental File Legends

File S1 A ±45° 3D projection of a representative wild type cell during early PSM growth. A 3D-projection was generated from a z-stack captured from early stage wild type (LH917) PSM development. PSMs were labeled with GFP-spo20$^{51-90}$ and histones were visualized with a genomically integrated *HTB2*-mCherry fusion.

File S2 A ±45° 3D projection of a representative *sps1Δ* cell during early PSM growth. A 3D-projection was generated from a z-stack captured from early stage *sps1Δ* (LH1047) PSM development. PSMs were labeled with GFP-spo20$^{51-90}$ and histones were visualized with a genomically integrated *HTB2*-mCherry fusion.

File S3 A ±45° 3D projection of a representative *spo77Δ* cell during early PSM growth. A 3D-projection was generated from a z-stack captured from early stage *spo77Δ* (LH1049) PSM development. PSMs were labeled with GFP-spo20$^{51-90}$ and histones were visualized with a genomically integrated *HTB2*-mCherry fusion.

File S4 A ±45° 3D projection of a representative wild type cell during late PSM development. A 3D-projection was generated from a z-stack captured from late stage wild type (LH917) PSM development. PSMs were labeled with GFP-spo20$^{51-90}$ and histones were visualized with a genomically integrated *HTB2*-mCherry fusion.

File S5 A ±45° 3D projection of a representative *sps1Δ* cell during late PSM development. A 3D-projection was generated from a z-stack captured from late stage *sps1Δ* (LH1047) PSM development. PSMs were labeled with GFP-spo20$^{51-90}$ and histones were visualized with a genomically integrated *HTB2*-mCherry fusion.

File S6 A ±45° 3D projection of a representative *spo77Δ* cell during late PSM development. A 3D-projection was generated from a z-stack captured from late stage *spo77Δ* (LH1049) PSM development. PSMs were labeled with GFP-spo20$^{51-90}$ and histones were visualized with a genomically integrated *HTB2*-mCherry fusion.

File S7 A time lapse video of a representative wild type cell (LH917) showing the normal closure kinetics of the PSM. Frames were captured in 2 minute intervals. Note that the tubular to rounded morphology transition spans approximately 2 minutes. PSMs were labeled with GFP-spo20$^{51-90}$ and histones were visualized with a genomically integrated *HTB2*-mCherry fusion. Note that the cell drifts from the left towards the right because of uncontrollable stage drift during the elapsed time of the experiment. Also, the prospore membranes disappear and reappear as they normally bobbed up and down within the cell out of the plane of focus in the z-axis.

File S8 A time lapse video of a representative *sps1Δ* cell (LH1047) showing the closure kinetics of the PSM. Frames were captured in 2 minute intervals. Note that the

tubular to rounded morphology transition spans approximately 40 minutes. PSMs were labeled with GFP-spo20$^{51-90}$ and histones were visualized with a genomically integrated *HTB2*-mCherry fusion. Note that the cell drifts from the upper right towards the bottom left because of uncontrollable stage drift during the elapsed time of the experiment.

File S9 A time lapse video of a representative *spo77Δ* cell (LH1049) showing the closure kinetics of the PSM. Frames were captured in 2 minute intervals. Note that the tubular to rounded morphology transition spans approximately 40 minutes. PSMs were labeled with GFP-spo20$^{51-90}$ and histones were visualized with a genomically integrated *HTB2*-mCherry fusion. Note that the cell drifts from the bottom left towards the upper right because of uncontrollable stage drift during the elapsed time of the experiment.